

Title page

Paper Type: Techniques and Resources article

Title: The buds of *Oscarella lobularis* (Porifera): a new convenient model for sponge cell and developmental biology.

Running title: A new model for sponge cell biology

Rocher Caroline ¹, Vernale Amélie ^{1,2}, Fierro-Constaín Laura ¹, Séjourné Nina ¹, Chenesseau Sandrine ¹, Marschal Christian ¹, Le Goff Emilie ³, Dutilleul Morgan ¹, Matthews Cédric ², Marschal Florent ¹, Brouilly Nicolas ², Massey-Harroche Dominique ², Ereskovsky Alexander ^{1,4,5}, Le Bivic André ^{2*}, Borchellini Carole ^{1*°}, Renard Emmanuelle ^{1,2*°}

1 : Aix Marseille Univ, CNRS, IRD, IMBE UMR 7263, Avignon Université, Institut Méditerranéen de Biodiversité et d’Ecologie marine et continentale, Station Marine d’Endoume, Marseille, France

2 : Aix Marseille Univ, CNRS, Institute of Developmental Biology of Marseille (IBDM), case 907, 13288, Marseille cedex 09, France

3 : ISEM, Université de Montpellier, CNRS, IRD, EPHE, Montpellier, France

4 : Saint-Petersburg State University, Saint-Petersburg, Russia

5 : Koltzov Institute of Developmental Biology of Russian Academy of Sciences, Moscow, Russia

*co-last authors

°co-Corresponding authors : Carole.borchellini@imbe.fr, Emmanuelle.renard@univ-amu.fr

Key words: morphogenesis, staining, imaging, culture, reproduction, regeneration

Summary statement: Studying sponge biology is needed to understand the evolution of metazoans. We developed a new model suitable for experimental biology that allows to study morphogenetic processes with modern tools.

Abstract: The comparative study of the four non-bilaterian phyla (Cnidaria, Placozoa, Ctenophora, Porifera) should provide insights into the origin of bilaterian traits. Except for Cnidaria, present knowledge on the cell biology and development of these animals is so far limited. Non-bilaterian models are needed to get further into cell architecture and molecular mechanisms.

Given the developmental, histological, ecological and genomic differences between the four sponge classes, we develop a new sponge model: the buds of the *Oscarella lobularis* (class Homoscleromorpha). This experimental model supplements the two other most famous sponge models *Amphimedon queenslandica* and *Ephydatia muelleri*, both belonging to the class Demospongiae.

Budding is a natural and spontaneous asexual reproduction mean, but budding can be triggered *in vitro* ensuring availability of biological material all year long. We provide a full description of buds, from their formation to their development into juveniles. Their transparency enables fluorescent and live imaging, and their abundance allows for experimental replicates. Moreover, regeneration and cell reaggregation capabilities provide interesting experimental morphogenetic contexts. The numerous techniques now mastered on these buds make it a new suitable sponge model.

55

56 **Introduction:**

57 Ctenophora and Porifera are currently the two best candidates as sister group of all other extant
58 animals (Daley and Antcliffe, 2019; Erives and Fritsch, 2019; Laumer et al., 2019; Simion et al.,
59 2017; Whelan et al., 2017). As a consequence, they can provide clues to understand the features
60 held by the last common ancestor of animals, the early evolution of animal body plans and the
61 origin of traits shared by bilaterians and cnidarians (King and Rokas, 2017; Schenkelaars et al.,
62 2019). Nevertheless, recent comparative studies evidenced that there are still many gaps in the
63 basic understanding of the cell and developmental biology of these animals (Dunn et al., 2015).
64 To fill in these knowledge gaps, the development of new biological models is required.

65 The most recent findings in sponge transcriptomics and genomics tend to conclude that gene
66 inventories are unable to explain the histological and morpho-anatomical differences found
67 either between sponge classes or between sponges and other animals (Renard et al., 2018).
68 Moreover, present knowledge in sponge cell and developmental biology mainly relies on
69 classical, static, optic and electron microscopy. Live, physiological and functional studies remain
70 very scarce until now (Adams et al., 2010; Borisenko et al., 2015; Ereskovsky et al., 2015;
71 Lapébie et al., 2009; Leys et al., 2011; Nickel, 2010; Rivera et al., 2011; Schenkelaars et al., 2016;
72 Lavrov et al., 2018). Physiological and functional data are therefore needed to finely describe
73 sponge cell characteristics and dynamics during morphogenetic processes.

74 Because of their histological, ecological, embryological differences and molecular divergence,
75 four sponge models should ideally be developed: one for each class, namely Demospongiae,
76 Hexactinellida, Calcarea, Homoscleromorpha (Renard et al., 2018). Currently, 13 genera and 16
77 sponge species are being studied at cellular and molecular levels for developmental biology
78 purposes (Schenkelaars et al., 2019) and represent “model organisms” in the historical sense
79 because they “are convenient to study a particular area of biology” (Russell et al., 2017). But,
80 to date, only one sponge species fulfills nearly all requirements to be considered a *bona fide*
81 “model organisms” in the modern sense (Russell et al., 2017), with a complete set of technical
82 tools and resources. This is the fresh water species *Ephydatia muelleri* for which functional
83 techniques are available (Hall et al., 2019; Rivera et al., 2011, 2013; Windsor Reid et al., 2018)
84 and easier to farm than most marine species. To study marine sponges, we therefore recently
85 developed a new biological resource, the bud of *Oscarella lobularis* (Schmidt, 1862) that fulfills
86 most of the criteria of a biological model, to explore the cell biology of a homoscleromorph
87 sponge. We believe this is a major step forward for sponge cell and developmental biology
88 research.

89 Homoscleromorph sponges are of particular interest to study the evolution of epithelia as it
90 has been already pointed (Belahbib et al., 2018; Boute et al., 1996; Ereskovsky et al., 2009,
91 2013b; Miller et al., 2018; Nichols et al., 2006, 2012) and the unexpected higher conservation
92 of some bilaterian genes in homoscleromorphs in comparison to other sponge classes was more
93 recently noticed (reviewed in Renard et al., 2018). Among Homoscleromorph sponges,
94 *Oscarella lobularis*, the type species of the Oscarellidae family, has benefited from in depth

studies of its histology, embryology and ecology (Ereskovsky, 2010; Ereskovsky et al., 2009). *O. lobularis* adults are commonly found on the rocky substrates of the north-western Mediterranean Sea. The discriminant features and phylogenetic relationships with respect to other homoscleromorph species has been previously studied (Gazave et al., 2010, 2012, 2013). This species is capable of both sexual and asexual reproduction by budding (Ereskovsky and Tokina, 2007; Ereskovsky et al., 2013a; Fierro-Constaín et al., 2017). To study cell and developmental biology of these animals we have previously developed techniques on the adult stage, available all year long in contrast to embryos: *in situ* hybridization (Gazave et al., 2008), pharmacological assays (Lapébie et al., 2009) and wound-healing experiments (Ereskovsky et al., 2015). Nevertheless experimenting on adults raises several issues: 1) the high number of natural specimens to be collected, 2) the dependence upon meteorological conditions to obtain samples, 3) the non-transparency of tissues (presence of pigments of different colors (Gazave et al., 2013; Gloeckner et al., 2013)) requiring to prepare histological paraffin sections to perform observation at the cellular level, which is neither compatible with the preservation of most antigens, nor with live imaging.

The present study shows how the natural properties of the bud of *Oscarella lobularis* and the technical tools that we developed on them make them a new, convenient and suitable biological resource for getting insights into sponge cellular features and processes occurring during morphogenetic processes. These resources and technical tools make the homoscleromorph sponge *O. lobularis* a very promising model organism.

Results

Budding is a natural process

A two-years *in situ* monitoring realized on six adults of a population of *Oscarella lobularis* from Marseille (43.212518° N, 5.330122° E) enabled us to monitor natural reproduction events and to complete the life cycle of this species (Fig. 1) (Fierro-Constain, 2016). We observed two types of asexual reproduction: by fragmentation (Fig. 1A) and by budding (Fig. 1B).

Asexual reproduction events occurred naturally several times during a year from October to April suggesting an exclusion of asexual and sexual reproduction in a same individual. Unlike sexual reproduction, fragmentation and budding do not seem to be synchronized between individuals. Budding events were observed at several periods at fall and early spring whereas fragmentation occurred at fall after the end of sexual reproduction (Fig. 1).

Description of the budding process and its triggering in vitro

Budding adults were first observed and sampled in the sea and the terminal steps of the budding process were monitored under laboratory conditions (Ereskovsky and Tokina, 2007). Similar budding can be triggered in the lab by a mechanical stress on adults all year long: by cutting collected adults in pieces (referred hereafter as fragments).

To monitor the whole budding process *in vitro*, 3 adults of *Oscarella lobularis* were sampled. Each individual was cut into 12 fragments. The mortality caused by this mechanical stress is significant (>50%). Indeed, all the fragments that originated from one of the three individuals died, whereas 17 (out of 24) fragments from the two other individuals survived. The following description is therefore based on the monitoring of these 17 fragments.

The budding process triggered *in vitro* can be divided into three steps (Fig. 2A; Table S1) that are identical to those previously observed during natural budding (Ereskovsky and Tokina, 2007):

- *Step 1*: is characterized by a transition from a smooth body surface to an irregular surface (upper pictures of Fig. 2A).
- *Step 2*: consists in the growth of branched finger-like protrusions. All the components of the adult tissue (exopinacoderm, endopinacoderm, mesohyl and choanoderm) are concerned by this process (Ereskovsky and Tokina, 2007).
- *Step 3*: consists in the swelling of the protruding tissues via the increase of the volume of their central cavity and in the tightening of their basal pole resulting in the formation of a short stalk (Ereskovsky and Tokina 2007).

Time-lapse imaging of the budding process (Movie 1) shows that 4 days after cutting, fragments continue to contract rhythmically as adults do (Nickel, 2010). Budding begins on the most external part of the fragment and move to the center of the fragment (centripetal progression) until only a shred of tissue remains.

The release of free buds starts 6 days after cutting and reaches a peak between 13th and 16th days after the beginning of budding process (Fig. 2B, Table S1). The efficiency of budding differs from one individual to another (Fig. 2C, Table S2), but one cm³ fragment of adult can produce a mean of 450 buds (Fig. 2D).

Bud morpho-anatomical features and development: from bud release to settled juvenile

Once free, the development of the bud can be subdivided into 4 morphologically distinct developmental stages (Fig. 3). The timing of occurrence of each stage is indicated in days since bud release (timing observed in standardized conditions). In other conditions (volume of natural sea water (NSW), frequency of sea water renewing, number of buds per well...) this developmental timing might be slightly different.

Stage 1 – just released spherical buds – Day 0.

At this stage, buds have a spherical shape. The central cavity is larger than it was before the release and larger than at next stages. This size ranges from 1 mm to 2.5 mm with a mean size of 1.87 mm (Fig. 2E). This difference of sizes can be explained both by a difference in the volume of the central cavity (diameter ranging from 160 to 700 µm) and by different levels of contraction between individuals (Movie 2). Indeed, buds keep on contracting rhythmically after their release from the adult tissue. These contractions are of different amplitude (Table S3): During a 105-min period, some buds can undergo a release up to 113% magnitude (mean: 53%, sd: 0,39).

The general tissue organization of the bud found around the central cavity is the same as in adult despite a simpler organization of the aquiferous system (Fig. 3A). The exopinacoderm forms the most external layer of the bud and is perforated by ostia (inhalant pores). The endopinacoderm lines the canals of the aquiferous system and the internal cavity. The choanoderm is composed of choanocyte chambers communicating with exhalant canals by apopyles. The chamber dimensions range from 36 to 52 µm (mean 44,7 µm, Table S4), a size range comparable to the smaller chambers observed in adults (Boury-Esnault et al., 1984).

Between these epithelial layers, the mesohyl, a mesenchymal layer, includes different cell types (next section) and symbiotic bacteria (the most abundant one being *Rhodobacter lobularis* (Jourda et al., 2015)).

Stage 2 – buds with outgrowths– Day 1 to Day 7.

The histological organization at stage 2 is similar to that observed at the first stage (Fig. 3B). The global shape becomes variable and asymmetric because of the formation of numerous external outgrowths. Outgrowths are only composed of exopinacoderm and

mesohyl. At their distal pole, roundish cells (absent or rare at stage 1) become obvious (Fig. 3B).

- *Stage 3 – buds with an osculum – Day 8 to Day 29.*

Stage 3 is characterized by the development of a polarized organization predating the basal-apical polarity of stage 4. On one pole (the future basal pole) the outgrowths are clustered, while at the opposite pole (the future apical pole), choanocyte chambers are clustered and an osculum develops (Fig. 3C). Larger choanocyte chambers are observed compared to stage 1 (up to 70µm large, Table S4, Fig. S1).

- *Stage 4 – juveniles settled on the substrate - from 1 month old.*

At stage 4 (Fig. 3D), buds attach to the substrate with the osculum pointing to the surface at the apical pole. The adhesion to the substrate is probably performed by the abundant mucus present at the distal parts of the outgrowths (Fig. 4B,F). These settled juveniles (with a reduced internal cavity or atrium) are similar to juveniles formed after larval metamorphosis (Ereskovsky and Tokina, 2007; Ereskovsky et al., 2007). Some stage 3 buds fail to settle, the unsettled buds can nevertheless stay alive for several months in culture plates.

In brief, the buds and the juvenile obtained *in vitro* present the same morphological and histological features than buds resulting from natural budding and the juveniles resulting from sexual reproduction.

Description of cell types

Previous histological description of buds at stage 1 (Ereskovsky and Tokina, 2007) reported that they are composed of the same 6 cell types as adults: exopinacocytes, endopinacocytes, choanocytes, apopylar cells, type I vacuolar cells and type II vacuolar/archaeocyte-like cells (Fierro-Constain et al., 2017). By using a combination of semi-thin histological sections, confocal microscopy and electron microscopy (TEM, SEM), we reassessed cell types (Figs 4, S2A-D).

Five epithelial cell types can be easily distinguished and fit the three key criteria defining epithelial cells (Leys et al., 2009; Renard et al., in press): a polarity made obvious by the presence of an apical flagellum (Figs 4A, S2B-D) and/or the abundance of basal actin-rich filopodia (Fig. S2A-C), actin-rich adherens-like junctions (Fig. S2C), and supported by a basement membrane containing type IV collagen (Figs S2B,C). All are covered externally by glycocalyx and mucus layers, the thickness of which can differ (Fig. 4 F,G). These epithelial cell types are:

- *Choanocytes:*

They form choanocyte chambers. Choanocytes are composed of a cellular body, an apical collar of microvilli and a flagellum composed of acetylated alpha-tubulin (Fig. 4A) and alpha-tubulin. The basal pole of choanocytes harbors long actin-rich cytoplasmic protrusions, filopodia, that pass through the basement membrane and contact other cells (Figs S2A,B).

- *Pinacocytes: endo-, exo- and basopinacocytes*

Endopinacocytes line inhalant and exhalant canals whereas exopinacocytes line external parts of the bud. Both have the same ovoid to flattened shape as in adults (Ereskovsky, 2010). The exopinacocytes possess one very long (up to 20 µm, Fig. 4A) flagellum, longer than that of endopinacocytes (5-10 µm). The acetylation of the alpha-tubulin composing the flagella of exopinacocytes is more heterogeneous than that of choanocytes with a spot-like distribution along the flagellum (Figs 4A, S2C,D). As for choanocytes both SEM 3D (Movie 3) and confocal imaging on whole mounted buds evidence long actin-rich expansions at the basal pole of this cell type passing through the basement membrane

and often contacting other cells (Figs S2A-C). Pinacocytes surrounding the ostia often present a fringe of actin protrusions at the edge of the pore (Fig. S2D) not reported so far. Both endo- and exopinacocytes contain more vacuoles than the ones found in adults (Ereskovsky et al., 2015). During the development of bud, round- to oval- shaped cells, with large vacuoles and very thick glycocalyx and mucus layers, are visible at the distal pole of the external outgrowths (Fig. 4B-F). These cells possess both short apical and long basal actin-rich cell extensions connecting with other cell types (Movie 4). Morphologically and functionally, these cells differ from the exopinacocytes, according to their position and putative function in bud settlement, we consider these cells as basopinacocytes, currently defined as pinacocytes affixing the sponge to the substratum by external secretion of a mucous layer (Boury-Esnault and Rützler, 1997; Ereskovsky, 2010).

- *Apopylar cell:*

This cell type forms the boundary of the opening of a choanocyte chamber into an exhalant canal or central cavity. They are characterized by a flat to triangular shape, a flagellum and microvilli at the apical pole (Fig. 4A).

Three mesenchymal amoeboid and motile (Movie 5) cell types can be distinguished (Fig.4A):

- *Type I vacuolar cell:*

They are characterized by the presence of 1 to 4 large electron translucent vacuoles with few short filopodia, the nucleus is localized laterally.

- *Type II vacuolar/archaeocyte-like cells:*

They have asymmetric amoeboid shape and are characterized by numerous vacuoles (empty or with fibrous inclusions, few osmiophilic inclusions), and the presence of few long actin-filopodia which often contact other cells.

- *Type III vacuolar cell type:*

The size of the cellular body ranges from 7 to 11µm. They harbor a clear polarity (in contrast to archaeocytes): one roundish pole and the opposite pole with numerous thin actin-rich filopodia (>5). As for archaeocytes, numerous vacuoles of different sizes are present in the cytoplasm.

In addition, we observed in the mesohyl numerous anucleate cell-like structures which size ranges from 2 to 5 µm: we interpret them as being extracellular vesicles (EVs) (Figs 4A, S2H,I) (Raposo and Stahl, 2019). EVs have various shapes spherical, ovoid or bean-shaped with an obvious actin-rich pole involved in motility capabilities. These EVs are probably microvesicles (MVs) according both to their size and because they seem to originate from budding at the basal pole of exopinacocytes (Fig. S2G).

In brief, according to the histological criteria, the buds of *Oscarella lobularis*, would harbor at least 8 cell types. Thanks to fluorescent confocal imaging, we evidenced the presence of two new cell types and of extracellular vesicles not described previously in this species neither in adults nor in buds (Ereskovsky et al., 2009; Ereskovsky and Tokina, 2007).

Bud are physiologically active individuals

Buds (stages 1 and 2 in particular) harbor a large central cavity allowing them to float in the water column, and flagella on the surface that, if motile, can participate to its mobility. Time laps imaging of the exopinacocytes flagella in white light, clearly shows their beating (Movie 6). We monitored the movement of fluorescent microbeads placed on the surface of

the exopinacoderm (Colibri imaging) in the presence or absence of nocodazole (Fig. S3). This preliminary experiment shows that flagella beating enables the directional movement of beads at the bud surface with a speed of about 47 $\mu\text{m/s}$. After 40 min of nocodazole treatment, a well-known microtubule inhibitor, the flux and the speed of beads drastically decreased. This observation shows that the particle flux and speed are directly correlated with the flagella beating.

In adult sponges, filtration is performed by the choanocytes which enable to pump the water unidirectionally through the body and phagocyte food particles (Renard et al., 2013). In order to establish if stage 1 buds are able to filter feed despite the absence of a complete aquiferous system, we compared the entrance of fluorescent microbeads (size 0.2 μm to mimic bacteria size) in the aquiferous system between Day 0 buds (stage 1, devoid of osculum) and Day 30 buds (stage 3 possessing an osculum) after 15, 30 and 60 min of incubation (Fig. 5). The localization of fluorescent microbeads in inhalant canals and choanocyte chamber cavities shows that stage 1 buds are capable of filtering (Fig. 5A). This process is fast: after only 15 min of incubation, beads were present in inhalant canals and in the cavity of choanocyte chambers, indicating that filtration started. After 30 min of incubation, beads were observed both at the level of the microvilli of choanocytes and in the cytoplasm of choanocytes (Fig. 5A), meaning they were phagocytized. However, the comparison between buds at stage 1 and 3 after 30 min incubation indicates that whereas all choanocytes contain beads in stage 3 buds, only some of them have accumulate beads in stage 1 buds (data not shown). Stage 1 buds are capable of filtration, but their filtering efficiency is lower than that of later stages. After 30 min in stage 3 buds, some mesohylar cells contain beads (Fig. 5B).

If buds are exposed to nocodazole before incubation with beads, no or hardly no beads are found in the aquiferous system (whatever the bud stage and the incubation time with beads) (Figs 5C, S4 for control). This observation shows that the filtering activity of buds (at all stages) is an active process depending on the beating of flagella, as for adults.

Morphogenetic processes and monitoring tools

Buds are suitable for experiments because they can be obtained in large amounts and their transparency (Movie 5) enables to stain and even track cells during morphogenetic processes. We adapted different detection and staining methods to evaluate key mechanisms (cell division, apoptosis and migration) in different developmental and non-developmental contexts.

Evaluation of cell renewing dynamics during bud development

To evaluate the rate of cell divisions and apoptosis events during bud development, we adapted usual approaches: Phospho-histone H3 (PHH3) immunolocalization as a marker of mitosis, 5-ethynyl-2'-deoxyuridine (EDU) cell proliferation assays and Terminal deoxynucleotidyl transferase dUTP nick end labeling (TUNEL) method for detecting DNA breaks generated during apoptosis.

According to PHH3 immunolocalization or EDU incorporation (Figs 6A,B, S5A,B) we found that about only 1% of cells divide at the same time (Fig. 6C, Tables S5,S6). Division occurs more frequently in choanocytes, and to a less extent in mesohyl cells than in other cell types (pinacocytes) (Figs 6A-C, S5A,B, Tables S5,S6). This may explain the slight increase of both the number of choanocytes per chamber and the size of choanocyte chambers between stage 1 and stage 3 (Table S4, Fig. S1).

TUNEL assays at different stages (Fig. 6D,E, Fig. S5D for control) shows that apoptotic cells represent between 10% (stage 3) and 16% (stage 1) of all cells (Fig. 6F, Table S7). Apoptosis is

heterogeneously distributed in buds and is observed more often in outgrowths. The cell types undergoing apoptosis are vacuolar cells and basopinacocytes (Fig. 6D,E). Interestingly, numerous extracellular vesicles are also stained (Fig. S5E). These results suggest that cell renewing (division/apoptosis balance) is low and slow during bud development.

To get insights into epithelial morphogenesis, we additionally developed regenerative and dissociation-reaggregation experiments that provide two complementary non-developmental contexts.

Wound healing and regeneration

Wound healing capabilities of *O. lobularis* adults have been previously studied (Ereskovsky et al., 2015). Here we show that stage 3 buds (harboring an osculum) are able of both wound healing and regeneration. Stage 3 buds (n=58) were cut into two parts: one part possessing outgrowths (future basal pole of the juvenile) and one part possessing the osculum (future apical pole of the juvenile). Of the 116 half-buds 100% survived to the injury. 24 h after the injury, both basal and apical halves successfully rescued the integrity of their external epithelium (exopinacoderm), or in other words, completed wound healing. In addition, 96% of the previously recovered halves can regenerate the missing part: an apical pole with a whole differentiated osculum or a basal pole with outgrowths, in 96 h or less (Fig. 7).

Reaggregation capabilities of dissociated cell

Bud cells can be efficiently dissociated by pooling thousands of buds (from a same adult) and stirring them in Calcium-Magnesium Free Sea artificial Water (CMFSW, supplemented in EDTA) as described for other sponge (Lavrov and Kosevich, 2014). A dense cell suspension (about $0.5 \cdot 10^6$ cells/mL) is thereby obtained (Fig. 8A). The viability of dissociated cells is high (>90%, data not shown).

The addition of calcium chlorid triggers cell reaggregation: 24 h after calcium adding, compact aggregates are obtained (Fig. 8B). Cell aggregation is followed by a neo-epithelialization: the surface of the aggregates becomes smooth. This stage is named primmorphs (Custodio et al., 1998): here, primmorphs are obtained within 48 h after calcium addition (Fig. 8C)

Monitoring cell migration during morphogenetic processes: Cell staining and tracking methods

To perform cell tracking during developmental and somatic morphological processes, we have developed three methods enabling to specifically stain and track choanocytes (Fig. 9):

- As previously shown, incubating buds with fluorescent beads for 30 min result in the engulfment of the beads by choanocytes. This method can be used to label choanocytes.
 - As described in *Amphimedon queenslandica* (Nakanishi et al., 2014), the lipophilic marker CMDil only stains choanocytes (Fig. 9A).
 - Among different tested fluorescent labeled lectins on alive buds, two lectins, GSL1 (*Griffonia simplicifolia* lectin 1) and PhaE (*Phaseolus vulgaris* Erythroagglutinin) stain specifically choanocytes, while accumulating in different sub-cellular structures (Fig. 9B,C). The long-lasting staining of choanocytes by these fluorescent lectins (up to 1 week) provides a convenient way to track these cells. For instance, using this method, we evidenced the migration of choanocytes to the mesohyl both during the natural development of bud and during preliminary regenerative experiments (Fig. 9D)
- Pinacocytes can also be stained by short (15-20 min) incubations with the wheat germ agglutinin (WGA, dilution 1:6000). Staining of only exopinacocytes or both endo- and

exopinacocytes depends on the incubation time (Fig. 9E). The obtained staining is much less specific than the ones mentioned for choanocytes because staining of other cell types is observed quickly when increasing incubation time (>20 min) or concentration (dilution <1:6000). The use of this staining therefore requires precision and careful stain checking before undergoing tracking experiments.

Towards functional approaches

We tested several methods (electroporation, lipofectamine and mannitol-based transfection reagents and simple soaking) to transfect three types of nucleic acids (plasmid, siRNA and morpholino). For plasmid (pmaxGFPTM Vector), none of the tested methods resulted in the expression of GFP and thus we were not able to ascertain its accumulation in the cells. In contrast, fluorescent siRNA block-it and morpholino (control) molecules were successfully transfected in choanocytes by simple soaking in artificial sea water (ASW) (Fig. 10). In these two cases, neither electroporation nor the addition of mannitol improved transfection efficiency. The localization of these fluorescent synthetic nucleic acids differs: siRNA are localized in vacuoles whereas morpholinos display a more homogenous distribution in the cytoplasm. Exopinacocytes also incorporate to a less extent the morpholino (Fig. 10D).

Discussion

The limits of cell type definition

In the literature, according to light and electron microscopies observations, the number of cell types described in sponges ranges from 6 to at least 16 (Ereskovsky, 2010; Simpson, 1984). Our observations using fluorescent confocal imaging on whole mounted buds of *Oscarella lobularis*, enabling Z-stacking and 3D projections, yielded to the description of additional cell types in comparison to previous data on the same stage (Ereskovsky and Tokina, 2007). The distinction between cells is thus highly dependent on the technique used. A complete reevaluation of cell types with complementary tools should therefore be launched in different sponge species.

Moreover, the distinction between cell types appears in part subjective. For instance, despite a developed actin fringe on the cells surrounding the ostia (Fig. S2D), in contrast to other pinacocytes, these cells have never been considered as a distinct cell type.

Finally, considering the disparity of terminology sometimes used for similar cells, the homology of these cell types between different sponge species is unclear.

It is therefore obvious that sponge cell biology expects much of the development of single cell transcriptomic approaches, enabling to define cell types on the basis of shared regulatory networks (Arendt et al., 2016). Such data was recently acquired for two demosponge species: *Amphimedon queenslandica* (Sebé-Pedrós et al., 2018; Sogabe et al., 2019; Wong et al., 2019) and *Spongilla lacustris* (Musser et al., 2019). These first results tell us more about cell functions in sponges and evidence different sub populations in a cell type (example choanocytes) enabling to discriminate more cell types (clusters) than previously thought. We guess that the present increased number of cell types recognized in *O. lobularis* buds (8-9 instead of 6) will soon be made obsolete by ongoing single cell transcriptomic approaches.

Two potential means of cell-cell communication in sponges

The capability of sponges to react to external chemical or mechanical stimuli has been thoroughly documented (Elliott and Leys, 2007; Leys, 2015; Leys and Meech, 2006; Leys et al., 2019; Mah and Leys, 2017; Maldonado, 2006; Nickel, 2010; Renard et al., 2009). A few sensory

cells were identified: such as light sensing pigmented cells of larvae (Collin et al., 2010; Leys and Degnan, 2001; Leys et al., 2002; Maldonado et al., 2003) or mechanical-sensory ciliated cells on adult osculum (Ludeman et al., 2014). A few effector cells were also identified such as pinacocytes and apopylar cells (Elliott and Leys, 2010; Hammel and Nickel, 2014; Ludeman et al., 2014; Nickel et al., 2011). In contrast, the mechanisms of cell-cell communication and signal transduction remain unclear though electric and chemical transduction were described: action potentials in Hexactinellida (Leys et al., 1999) and neurotransmitters in demosponges (Elliott and Leys, 2010; Ellwanger and Nickel, 2006; Ellwanger et al., 2007).

Here, we observed for the first time in the homoscleromorph class the impressive length that filopodia can reach, resulting in the establishment of a real network between pinacoderm, mesohylar cells and choanoderm. These filopodia are likely to be a key element of cell-cell communication in these sponges. The significance of such cell-cell contacts was also very recently observed in *Spongilla lacustris* (Musser et al., 2019). It is possible that the existence of such a developed cell-cell interacting network was underestimated because of the common use of sections to study sponge anatomy.

Moreover, we observed microvesicles (MVs), a subtype of extracellular vesicles (EVs) (Raposo and Stoorvogel, 2013) in the mesohyl of *O. lobularis* buds. Though similar structures were previously observed in other sponge species, they were not identified as EVs: “bubbles” formed by cell shedding in another homoscleromorph sponge (Ereskovsky et al., 2007) supposed to regulate cell shape and size; and “small anucleate nurse cells” involved in the oogenesis of *Chondrilla* (Maldonado et al., 2005). The understanding of the significance of EVs in cell-cell communication in Eukaryotes including animals is recent (Mulcahy et al., 2014). It is now obvious that such microvesicles can be used to carry nucleic acids (DNA, miRNA), proteins (transcription factors) from one cell to another, can participate to immune response (antigen presentation, cell-symbiont interaction), and to apoptosis mechanisms... (Latifkar et al., 2019; Margolis and Sadovsky, 2019; Niel et al., 2018; Raposo and Stahl, 2019). Here, the TUNEL staining of some of the MVs suggests that at least some of them are apoptotic extracellular vesicles (ApoEVs), also called apoptotic bodies, supposed to play a central role in immune modulation by dying cells (Caruso and Poon, 2018). Additional studies are now needed to confirm the nature of these vesicles and evaluate their roles in cell-cell communication in sponges.

Our findings therefore represent an important step forward for the understanding of cell-cell communication mechanisms in sponges.

Significant prospects for morphogenetic studies in sponges

The capability of dissociated sponge cells to reaggregate has been reported decades ago (Lavrov and Kosevich, 2014, 2016; Simpson, 1984).

As far as we know, dissociation-reaggregation has not been evidenced so far in homoscleromorph species (Grice et al., 2017). This study is thereby the first report of successful dissociation-reaggregation experiments in this class. This process offers a convenient experimental context to understand the molecular and cellular mechanisms involved in self/non-self-recognition (Grice et al., 2017) and in cell adhesion. Because Homoscleromorpha is the only sponge class with obvious basement membrane and adherens-like junctions, this simple experimental set-up provides the opportunity to study the dynamics of formation of these key structures of animal epithelia in early metazoans.

Moreover, the resulting primmorph can be considered as a 3D cell-culture system (Rady et al., 2019), which can be useful considering the difficulties to establish sponge cell cultures (Conkling et al., 2019).

The second somatic morphogenetic process reported here in *O. lobularis* is regeneration that offers the possibility of regenerative experiments. Most experiments performed on sponges (including the adults of *O. lobularis*, Ereskovsky et al., 2015; Fierro-Constaín et al., 2017) are wound-healing experiments instead of regenerative experiments (Lavrov et al., 2018). Indeed, the authors focus on the restoration of exopinacoderm integrity. Here we performed regenerative studies on buds by cutting off a key functional structure of sponges: the osculum. It is well-known that wound-healing and regenerative capabilities are highly variable from one animal phylum to another. Therefore, the origin and evolution of these properties (homologous or homoplastic features) is still debated (Lai and Aboobaker, 2018). The reproducible and quick osculum regeneration in buds of *O. lobularis* provides a simple and convenient model to study cellular and molecular mechanisms involved during sponge regeneration.

Launching knock down assays

The last decade of evo-devo studies on sponges was dedicated mostly to the acquisition of transcriptomic and genomic data. These significant data have highlighted the conservation of most of the main genes involved in developmental processes of the other metazoans. The next step is to understand how similar genetic toolboxes can result in dissimilar body organization and features. To answer this question, three main axes of research have to be undertaken: increasing gene expression studies; reinterpreting sponge cell biology (previous section); and developing knock down protocols. Interfering with gene expression is required to study gene functions, but it undoubtedly the biggest challenge for sponge biology (Lanna, 2015; Schenkelaars et al., 2019).

So far, efficient and reproducible transfection and interference was only used in the freshwater demosponge *Ephydatia muelleri* (Hall et al., 2019; Rivera et al., 2011, 2013; Windsor Reid et al., 2018). Four other papers report gene transfection assays in other sponges : one in another freshwater species *Spongilla lacustris* and three in marine demosponge species (Grasela et al., 2012; Pfannkuchen and Brümmer, 2009; Revilla-I-Domingo et al., 2018; Rivera et al., 2011). Unfortunately, transfections either failed or their efficiency was too low to perform reliable knock-in or knock-down. One of the difficulties is probably that most marine sponges tolerate only low salinity changes. Altering the salinity of media (for RNA stability or electroporation purposes for example) remains a major challenge for the future.

Here, we report the first tests of transfection in a homoscleromorph species, even if many conditions (types of plasmids, promoters, transfection reagents, choice of targets...) remain to be tested. The efficient and reproducible incorporation of fluorescent-standard control morpholino in the cytoplasm of choanocytes (with a homogenous distribution) is a first encouraging step. Indeed, these synthetic nucleic acids are well known for their high stability and have already been used successfully in marine species (Heasman, 2002). Nonetheless, at this point, we cannot presuppose the ability of these transfected molecules to efficiently interfere with gene expression or translation in this species.

Oscarella lobularis reaches the top 3 of sponge “models”

The embryology, life cycle, development, regeneration, histology of the homoscleromorph sponge *Oscarella lobularis* are well described. Moreover, its genome annotation and single cell transcriptomic are in progress to complete this knowledge (Belahbib et al., 2018; Jourda et al.,

2015). Like other species, *O. lobularis* reproduces both sexually and asexually. We managed to artificially induce in the lab a natural asexual reproduction event: budding, that occurs several times a year in natural conditions.

The buds obtained from *O. lobularis* are numerous and easy to maintain several months in the laboratory in natural sea water or up to one week in artificial sea water and can travel for up to 10h. These buds therefore offer the possibility of performing a wide range of assays (on individuals either genetically identical or not). Buds are small so that incubation in small volumes is possible (100 µL) which is convenient for expensive or toxic reagents. Moreover, in contrast to gemmules, a dormant stage produced in freshwater sponges (Simpson, 1984), *Oscarella* buds are physiologically active and can be used for physiological assays.

Buds are transparent therefore enabling fluorescent imaging on both fixed and live specimens. The present paper is also the first report of the use of fluorescent lectins for specific cell labeling in sponges. This is a significant step forward for cell tracking experiments to evaluate transdifferentiation events. We now also master usual tools to study cell migration, cell proliferation or apoptosis during the natural development of buds but also during regeneration and dissociation-reaggregation experiments.

Altogether, these technical progresses in *Oscarella lobularis* buds provide new tools to better understand sponge cell biology and the cellular and molecular mechanisms involved in this sponge class. The variety of experimental tools available will establish *O. lobularis* buds as a biological model comparable to that of the juveniles of the demosponge *Amphimedon queenslandica*, and the freshwater species *Ephydatia muelleri* (table 1).

Though sponges have been studied for over a century, the main sponge “models” (Lanna, 2015; Russell et al., 2017) according to the availability of data and techniques belong to the demosponges. The emergence of a new biological resource pertaining to a distinct class, i.e. the buds of *Oscarella lobularis* (Homoscleromorpha), is highly significant for evo-devo comparative approaches (Renard et al., 2018). Moreover, because of the features of homoscleromorph epithelia compared to that of the other sponge classes, this model is of particular interest to study the evolution of epithelia and epithelial morphogenesis.

Material and methods

In situ life cycle monitoring

The *in situ* monitoring of a small population in the bay of Marseille (western Mediterranean Sea) was carried out. Six adults of different sizes and colors located on the north edge of Maïre Island (43.212518 ° N, 5.330122 ° E), in a large, shallow and rocky cavity (6-10 m). The photographic monitoring was implanted once a month from April 2014 until October 2015. In addition, a small fragment of each individual was sampled twice a month, and fixed (in 4% PFA overnight (O/N)). Histological observations and *in situ* hybridization were realized on sections of these small fragments (Fierro-Constaïn et al., 2017) to determine the beginning and end of the sexual reproduction period. Sampling compliance provided by the “Préfet de la région PACA”.

In vitro budding and maintain of buds in lab conditions

Freshly collected Adults (in the northwestern Mediterranean Sea (Marseille Bay)) are carefully cleaned under stereomicroscope to get rid of other organisms intermingled with sponge tissues (cnidarians, annelid tubes, algae). Then, samples are cut into pieces of about 1 cm³ with a sterile scalpel. Each fragment is placed in a well (3.5 cm diameter) of a 6 wells cell culture plate

569 containing 8 mL of natural sea water (NSW). Culture plates are maintained at 17°C in a
570 thermostated room, NSW is renewed each day until the end of budding.
571 Once buds are released from the adult fragment, they are transferred to Petri dishes (14 cm
572 diameter) containing NSW and maintained at 17°C. NSW is renewed once a week.
573 To estimate the efficiency of budding *in vitro*, 3 adults of *Oscarella lobularis* sampled *in situ* in
574 January 2018 were placed in thermostated room at 17°C overnight (ON), before starting
575 experiment. Budding experiment was performed as described above. Each sample was cut into
576 12 fragments. Samples were observed and imaged, and buds counted every day. The bud
577 production per day was analyzed using linear mixed effects models (LMM) that were
578 implemented within lme4 package in the R software (Core Team, 2013). We considered time as
579 fixed effects and we allowed linear and/or quadratic effects on the dependent variable. We also
580 added individuals (with random slope of time within individuals) and replicates (fragments)
581 nested in individuals as random effects.
582 After observation of the residual's distribution of the models, we retained Gaussian
583 distribution. We tested the significance of fixed and random effects respectively with *F* tests
584 and likelihood ratio tests. When two models were equivalent, we retained the most
585 parsimonious model.

586

587

588 ***TL Photonic, SEM and TEM microscopy observations of budding adults and buds***

589 For scanning (SEM), transmission (TEM) electron microscopy and semi-thin sections'
590 preparation a standard fixation method for TEM was used: glutaraldehyde 2.5 % in a mixture of
591 0.4M cacodylate buffer and seawater (1 vol., 4 vol., 5 vol., 1,120 mOsm) and post-fixation in 2%
592 OsO₄ in sea water as first described in Boury-Esnault et al. (1984). Semi-thin sections were
593 stained with toluidine blue. For SEM the specimens were fractured in liquid nitrogen,
594 critical-point-dried, sputter-coated with gold-palladium according to the protocol previously
595 used for this species (Johnston and Hildemann, 1982).

596

597 ***Observation of mucus on buds' surface***

598 Buds were fixed in 3% paraformaldehyde (PFA) in phosphate buffered saline (PBS) at 4°C ON,
599 then washed 3 times with 1mL of PBS (15 mins each) at room temperature (RT). Buds were then
600 incubated 10 min in 1mL of Alcian Blue solution (Alcian Blue 1% in Acetic Acid 3%, pH 2.5)
601 (20:1000 in NSW) at RT, rinsed in 2 baths with NSW and immediately mounted with ProLong®
602 Antifade Mountant. After polymerization (40 min at 37°C in obscurity) the samples were
603 observed with a stereomicroscope.

604 For TEM observations, we used a special fixation with ruthenium red (Ereskovsky, personal
605 communication). Buds were fixed in buffered 2.5% glutaraldehyde + 0.1% ruthenium red for 2
606 h at 4°C, then rinsed 3 times with the 0.1M Na-Cacodylate buffer (30 min each) at RT, post-
607 fixation in buffered 1% OsO₄ + 0.1% ruthenium red in the same buffer for 3 h at RT, then rinsed
608 3 times with the same buffer (30 min each) at RT, dehydration in ethanol series and inclusion
609 in a resin.

610

611 ***Immunofluorescent assays on whole bud***

612 Buds are usually fixed (6 h to 24 h) in 3% paraformaldehyde (PFA) in PBS at 4°C.
613 After fixation, buds were washed in three baths of PBS (15 min each), then, buds were
614 incubated 45 mins in a blocking solution (Blocking Reagent (BR) (Roche) at 2% and saponine
615 (Sigma) at 0.1% in PBS). Incubation with primary antibodies (against acetylated- α -tubulin
616 (Sigma) (1:500), α tubulin (Sigma) (1:500), or type IV collagen (Eurogentec) (1:200)) was

performed in a blocking solution at 4°C ON. Buds were washed in 3 baths of PBS (5 min each) at RT. Buds were incubated at RT for 1 h with Alexa Fluor-coupled secondary antibodies (1:500 in PBS) (anti-mouse or anti-rabbit (Jackson ImmunoResearch or LifeTechnologies)). After counterstaining with Alexa fluor-(488, 568 or 647) coupled- phalloidin (1:1000; Thermo Fisher Scientific or Santa Cruz Biotechnology) and DAPI at 2 mg/mL stock solution (1:500) 15 min in PBS, samples were rinsed and mounted in ProLong™ Diamond Antifade Mountant or ProLong™ Gold Antifade Mountant (Invitrogen).

Homemade antibodies against the type IV collagen of *O. lobularis* were targeted against the QTISDPGEEDPPVSKC peptide from the NC-1 domain (GWLLVVHSQTTDLPCPDGSAMLYSGYSFLQSLGNGYGHGQDLGRPGSCLRVFSTMPFMHCSSSQCLVA ERSDISYWLTDDQVMPVNQEDDDGNIAKYISRCAVCETKSRTIAVHNQSTGVPDCPRGWDSVWQGFSFI AQTNDGAEGGGQSLSSPGSCLRRFYPMPYIECYPRGNCKYSSPGLSFWLSPLDDTEPPFDPPVRQTISDPGE EDPPVSKCRVCSKR). They were raised in rabbits using the speedy protocol from Eurogentec (Seraing, Belgium) and purified against the same peptide before using for immunofluorescence at 1:200.

Imaging of tissues and cells were performed with an inverted confocal microscope Zeiss Axiovert 200M or confocal microscope Zeiss Axio Imager Z2 780 or 880 (objective X63-NA 1.4). The FIJI software (Schindelin et al., 2012) was used for images editing (crop, color balance, choice of colors, z-stacking, 3D projection).

SEM3D observations of buds

Samples were prepared using the NCMIR protocol for SBF-SEM (Deerinck et al., 2010). Imaging was carried out on a FEI Teneo VS running in low vacuum (30 Pa), at 2kV and using a backscattered electrons detector. Acquisition voxel size was 5x5x40 nm.

Time Laps imaging of budding, buds and cells

For the time-lapse imaging of the budding process, adult fragments in 6 well cell culture plate containing 8 mL natural sea water (NSW), were placed in a dark chamber at 17°C. We used a CANON EOS 750D camera with an EF-S 60mm 1/2.8 1:2.8 USM *Ultrasonic Macro Lens* to acquire one picture every 15 min during 6 days.

We used the same protocol for imaging the contractions of the free buds *in vitro*, in this case the time-lapse imaging was performed by taking one picture every 5 min for 48 h. For each bud, the maximum and the minimum sizes were measured in pixel to evaluate the amplitude of bud contraction/release. The mean and the standard-deviation (sd) were calculated on the R software (<https://www.r-project.org/>).

To observe cell motility, time-lapse imaging was performed on a stage 3 bud placed into 6 wells cell culture plate with natural sea water, at 22°C. We used an inverted microscope Zeiss Axio Observer Z1 in DIC TL, with an objective X20-NA 0.7, to acquire one picture every 10 s during 10 min (total 61 pictures).

To observe cilia beating on the exopinacoderm, a time-lapse imaging was performed on a bud with a microscope Zeiss Axio Imager Z1 with DIC II (objective X40-NA 1.3) with a rate of one picture every 34.3 ms during 30 sec.

Testing Filtering and cilia activities with fluorescent beads

Day 0 (stage 1) and Day 30 (stage 3) 10 buds were incubated 15 min, 30 min and 1 h with 0.2µm FluoSpheres™ Carboxylate-Modified Microspheres yellow-green (505/515nm) (Molecular Probes) in 2 mL (1/10000) of NSW at 17°C. Buds were then rinsed 3 times with NSW and fixed (3% PFA) at 4°C ON. After DAPI/ Phalloidin counterstaining and mounting as described in the previous section, imaging of samples was performed with a confocal microscope Zeiss LSM 880 Leica. The same experiment was reiterated after a 40 min nocodazole (33µM) treatment (nocodazole is an inhibitor of tubulin polymerization, process required for cilia beating). As a control, buds were incubated 40 min in a DMSO solution (1/1000, the same concentration as the one used to solubilize nocodazole).

To characterize the beating of exopinacoderm cilia, buds were incubated with 0.5µm FluoSpheres™ Carboxylate-Modified Microspheres Red (580/ 605nm) in a Petri dish with a coverslip. The movement of fluorescent beads in live, was imaged with an inverted optical microscope Axio Observer Z1 with a LED system illumination (Zeiss). In order to estimate the flow created by cilia, the path of the beads was measured with Fiji plugin “Track Mate” with “DoG detector” and “LAP tracker” options. The same experiment was reiterated after a 40 min nocodazole (33µM) treatment.

TUNEL assays

Buds were fixed 20 min with 3.7% PFA in filtered seawater and then permeabilized for 20 min at RT with 0.2% Triton X-100 in TS solution (150 mM NaCl, 25 mM Tris, pH 7.5). After rinses, TUNEL staining (Roche, *In situ* cell death rhodamin detection kit) was performed according to the manufacturer's instructions. Nuclei were detected with DAPI labelling (Euromedex). Samples were analyzed with a confocal microscope Leica TCS-SPE (Montpellier RIO Imaging platform, France). The number of nuclei and stained nuclei (table S6) was estimated using FIJI cell counter. A statistical analyze with R is performed using the Kruskal-Wallis test follow by a Dunn test.

Cell proliferation assays

Cell division activity was estimated on both young (stage 1, 0-3 days old) and older buds (stage 3, 1 month old) by two different means: anti Phospho-histone H3 (PHH3) immunolocalization (Abcam ab5176) antibody (1:200) (see previous section for details on immunofluorescent assay protocol) and EDU staining. EDU staining was performed according to manufacturer recommendations (Click-iT™ and Click-iT™ Plus EDU Alexa Fluor™ 488 Imaging Kit (Invitrogen). Assays were performed with 10 µM, 50 µM and 200 µM in NSW: the optimal concentration was then fixed to 50 µM. Assays were performed in 24 well culture plates, each plate containing 1mL of 50µM EDU solution. Buds were incubated for 2, 6 or 24 h at 17°C. Only 6 h and 12 h incubation times yielded suitable results. Observations were performed with optical sectioning systems: an apotome microscope Axio Imager Z1 (EDU) or confocal microscope Zeiss Axio Imager Z2 780 (PHH3). The number of nuclei and stained nuclei (tables S4 and S5) was estimated using FIJI cell counter. A statistical analyze with R is performed using a one factor Anova.

Regenerative experiments

Stage 3 buds (n=58, 3 independent technical replicates), with a differentiated osculum, were cut into two halves: one half corresponding to the future basal pole of the juvenile, and one half possessing the osculum and corresponding to the future apical pole of the juvenile (Fig.7). The 116 half-buds obtained after cutting) are placed in 24-wells culture plates containing 2mL

of Natural Sea Water (NSW, renewed every day), and the culture plate placed at 17°C. Wound healing and regeneration were monitored once a day during 96 h. Two additional preliminary experiments consisted in staining choanocytes with the PhaE lectin (as in next section) before cutting in order to evaluate choanocyte migration during the regenerative process.

Cell dissociation-reaggregation experiments

Thousands of buds were collected in a Falcon tube (15mL) then slowly centrifuged, 10G 2min at RT. The supernatant of natural sea water (NSW) was discarded and the bud solution (1.5mL) was incubated in 20mL Calcium Magnesium Free Sea Water (CMSFW: 0.54 M NaCl, 10 mM KCl, 7 mM Na₂SO₄, 15 mM tris-HCl, 0.2mM NaHCO₃, pH8) with 10mM EDTA pH8 and stirred for 1 h at RT. Cell suspension was filtered on 17 µm cell strainer. Concentration of cellular suspension was evaluated using C-Chip Neubauer. Before counting, the viability of cells, can be efficiently evaluated with fluorescein diacetate (FDA) and propidium iodide (PI) staining (Sigma) according to the protocol used by Sipkema et al. (2004).Then, 2mL of cell suspension (between 0.4.10⁶ and 0.56.10⁶ Cells/mL) were dispatched in 24 wells cell culture plate and CaCl₂ solution was added to each well (final concentration 20mM). Culture plate was placed at 17°C and stirred very slowly on a 3D platform shaker. After reaggregation, cell aggregates were thus carefully transferred in 2mL Artificial Sea Water (ASW: 10mM CaCl₂, 50mM MgCl₂, 6H₂O, 0.54M NaCl, 10 mM KCl, 7 mM Na₂SO₄, 15 mM tris-HCl, 0.2mM NaHCO₃, pH 8) in 6 wells cell culture plates. Culture plates are placed at 17°C and stirred very slowly on a 3D platform shaker. The reaggregation process was monitored during 7 days. This manipulation has been repeated 3 times.

Cell staining

Stock solution (1 mM) of the lipidic marker Cell Tracker™ CM-Dil Dye Red (553/570nm) (Molecular Probes) was prepared in dimethylsulfoxyde solution (DMSO). After short centrifugation, 2 µL were introduced in 1 mL NSW (1:500) and transferred in 24 wells cell plate with buds at 17°C ON.

All fluorescent (rhodamine or fluorescein labeled) lectins and agglutinins provided in vector laboratories kits (kit I (RLK-2200), kit II (FLK-3200) and kit III (FLK-4100)) were tested at different concentrations (1:100, 1:500, 1:1000, 1:2000 in NSW) for 15 min, 30min, 1 h at 17°C. After each treatment, buds were rinsed three times in NSW and immediately observed with an epifluorescence microscope DM2500 Leica and a confocal zeiss lsm 510 (for CM-Dil Dye treatment).

In a second step, the dilution and incubation times were optimized, for the 3 lectins that showed a more specific pattern: *Griffonia simplex* lectin 1 (Gsl1), *Phaseolus vulgaris* Erythroagglutinin (PhaE) and *Wheat germ agglutinin* (WGA).

For more precise observations samples were fixed with 3% PFA/PBS at 4°C ON, counterstaining with DAPI (1:500) (Thermo Fisher Scientific) and 1:1000 (iFluor 488 or Rhodamine or Alexa- 647 (or 568) coupled-) phalloidin (Abcam, Thermo Fisher Scientific) and mounted in Prolong Diamond antifading mounting medium (Thermo Fisher Scientific); and then observed with confocal microscope Zeiss AxioImager Z2 780 or 880.

Cell transfections

To develop a cell transfection protocol, we first used control nucleic acids molecules (BLOCK-iT™ Fluorescent oligo control (Invitrogen™), pmaxGFP™ Vector (expressed under a CMV-

760 promoter; LONZA) and a morpholino standard control oligo (Gene tools) with 3' carboxy-
761 fluorescein green, in order to test transfection efficiency.

762 For soaking method, BLOCK-iT™ fluorescent oligo (20μM stock) were used at different final
763 concentrations (2nM, 4nM, 8nM, 100nM) and pmaxGFP™ Vector (0.5μg/μL stock) at 5μg and
764 30μg in 5 mL natural sea water (NSW). Then, 3-5 buds were directly put in contact with these
765 solutions placed of a 6 well cell culture plate and maintained at 17°C during 5H, 16H, 24H,
766 48H,72H, 5 days or 7 days without changing the sea water. The buds were rinsed 3 times with
767 NSW and then observed with an epifluorescence microscope Leica DM2500 and a confocal
768 microscope Zeiss after fixation and mounting.

769 For standard control morpholino (1mM stock) we tested different concentrations (10μM, 1μM,
770 0.9μM, 0,8μM, 0,6μM, 0,5μM and 0,1μm) in 500μL (filtered or not) NSW. The buds were placed
771 in a 24 well cell plate (4 buds per well) and incubated at 17°C with the morpholino solutions
772 during 24H, 48H, 72H, 96H and 120H. The buds were rinsed 1 time with NSW and fixed in PFA
773 3% O/N at 4°C. Alive buds were observed with an epifluorescence microscope Leica DM2500,
774 and after counterstaining and mounting observed the samples with a confocal microscope
775 Zeiss.

776

777 For testing the efficiency of lipofection for pmaxGFP™ Vector and BLOCK-iT™ fluorescent oligo,
778 two lipofectamine transfection reagent (Invitrogen™), Lipofectamine® 3000 and
779 Lipofectamine® LTX DNA (less cytotoxic) were tested in this study according the “24-well”
780 protocol of the manufacturer’s instructions using 1μg DNA, but replacing the Opti-MEM™
781 medium, shown to be toxic for the buds by preliminary experiments, by PBS or filtered NSW.
782 We used the indicated volume of DNA and reagent with each of the volume lipofectamine™
783 3000 or LTX as preconized when performing optimization. Buds (N=24 for Lipofectamine® 3000;
784 N=60 for Lipofectamine® LTX DNA for each of DNA constructs) were incubated at 17°C during 1
785 to 2 days and then rinsed with NSW before observation with an epifluorescence microscope
786 DM2500 Leica. For morpholino standard control oligo, the different concentrations, as
787 described above, were tested with aqueous (mannitol-based) Endo Porter solution at 1μM,
788 2μM, 3μM and 6μM in 500μL NSW. The buds are treated in the same conditions as without
789 EndoPorter (see above).

790

791 We also tested electroporation method for BLOCK-iT™ fluorescent oligo and pmaxGFP™ Vector
792 introduction in *O. lobularis* cells using the Neon™ Transfection System and Neon™ Tip 100μL
793 (Invitrogen). To avoid electric arcs, we replaced NSW by a Mannitol solution (0,77M) (Zeller et
794 al., 2006). We used 6μg to 15μg of pmaxGFP™ Vector (0.5μg/μL stock) and 0.1 to 0.2μM of
795 BLOCK-iT™ (20μM stock) for each electroporation. 14 buds were added to the Mannitol solution
796 (120μL) with or without acids nucleic molecules and incubated 1 min. Then the mixture was
797 transferred into tips and electroporated at different conditions (0 Volt-1mS-1 pulse / 500 volts-
798 1mS-1 pulse /500volts-5mS-1pulse /500 volts-40mS-1pulse / 500 volts-1mS-5 pulses / 500V-
799 10mS-2 pulses / 500 volts-5mS-1pulse / optimization of Neon system number 5 / 7 / 10 / 13/18/
800 24). After electroporation, buds were placed in 6 mL NSW at 17°C (plate-6 wells) during 4, 24,
801 96, 120 or 168H before epifluorescence microscope observations.

802

803

804 **Acknowledgements**

805 All the authors thank the imaging facilities of the France Bioimaging infrastructure and in
806 particular Brice Detailleur, Laetitia Hudecek and Elsa Auroux-castellani for their help and
807 advices to develop imaging in *O. lobularis* buds. We also acknowledge the diving facilities of the

Institute OSU Pytheas (Frédéric Zuberer, Laurent Vanbostal and Dorian Guillemain) and divers from the IMBE lab (Anne Haguenauer, Pascal Mirleau) for *in situ* monitoring and collecting *O. lobularis*. We thank the molecular biology and morphology support services of IMBE for providing facilities needed to develop techniques. We also thank Elsa Bazellières for her help in launching bead monitoring and Jean Vacelet for helpful discussions.

We are grateful to Matthieu De La Rosa, Cassandra de Pao Mendonca, Damien Vary and Maxime Angely who participated in preliminary experimental assays during their internships.

Competing interests

No competing interests declared.

Funding

This work was funded by the Centre National de la recherche Scientifique (CNRS, UMR7263 and UMR7288) : project for international scientific cooperation (PICS) STraS involving CR, AE, SC, ER, CB, ELG, ALB, DMH, CM, AV), and also by the Aix-Marseille University and the A*MIDEX foundation project (n° ANR-11-IDEX-0001-02 to CB, ER, ALB, CR, NS, SC, CM and AE); ALB, DMH and NB are supported by the LabEx INFORM (ANR-11-LABX-0054) both funded by the «Investissements d’Avenir » French Government program, managed by the French National Research Agency (ANR)". The Russian Science Foundation, Grant n° 17-14-01089 (TEM studies) to AE. The region Sud/PACA and Aix-Marseille University are also acknowledged for the funding of respectively L. Fierro-Constaín and A. Vernale PhD fellowships. The light and electron microscopy experiments were performed on PiCSL-FBI core facility (IBDM, AMU-Marseille), member of the France-BioImaging national research infrastructure (ANR-10-INBS-04).

References

Adams, E. D. M., Goss, G. G. and Leys, S. P. (2010). Freshwater Sponges Have Functional, Sealing Epithelia with High Transepithelial Resistance and Negative Transepithelial Potential. *PLoS One* **5**.

Adamska, M., Degnan, S. M., Green, K. M., Adamski, M., Craigie, A., Larroux, C. and Degnan, B. M. (2007). Wnt and TGF-beta expression in the sponge *Amphimedon queenslandica* and the origin of metazoan embryonic patterning. *PLoS ONE* **2**, e1031.

Alié, A., Hayashi, T., Sugimura, I., Manuel, M., Sugano, W., Mano, A., Satoh, N., Agata, K. and Funayama, N. (2015). The ancestral gene repertoire of animal stem cells. *Proc Natl Acad Sci U S A* **112**, E7093–E7100.

Arendt, D., Musser, J. M., Baker, C. V. H., Bergman, A., Cepko, C., Erwin, D. H., Pavlicev, M., Schlosser, G., Widder, S., Laubichler, M. D., et al. (2016). The origin and evolution of cell types. *Nat. Rev. Genet.* **17**, 744–757.

Belahbib, H., Renard, E., Santini, S., Jourda, C., Claverie, J.-M., Borchellini, C. and Le Bivic, A. (2018). New genomic data and analyses challenge the traditional vision of animal epithelium evolution. *BMC Genomics* **19**, 393.

Borisenko, I. E., Adamska, M., Tokina, D. B. and Ereskovsky, A. V. (2015). Transdifferentiation is a driving force of regeneration in *Halisarca dujardini* (Demospongiae, Porifera). *PeerJ* **3**, e1211.

Boury-Esnault, N. and Rützler, K. (1997). *Thesaurus of sponge morphology*. Smithsonian Institution Press.

Boury-Esnault, N., Vos, L. D., Donadey, C. and Vacelet, J. (1984). Comparative study of the choanosome of Porifera: 1. The Homoscleromorpha. *Journal of Morphology* **180**, 3–17.

Boute, N., Exposito, J.-Y., Boury-Esnault, N., Vacelet, J., Noro, N., Miyazaki, K., Yoshizato, K. and Garrone, R. (1996). Type IV collagen in sponges, the missing link in basement membrane ubiquity*. *Biology of the Cell* **88**, 37–44.

858 **Caruso, S. and Poon, I. K. H.** (2018). Apoptotic Cell-Derived Extracellular Vesicles: More Than Just Debris.
859 *Front Immunol* **9**.

860 **Collin, R., Mobley, A. S., Lopez, L. B., Leys, S. P., Diaz, M. C. and Thacker, R. W.** (2010). Phototactic
861 responses of larvae from the marine sponges *Neopetrosia proxima* and *Xestospongia*
862 *bocatorensis* (Haplosclerida: Petrosiidae). *Invertebrate Biology* **129**, 121–128.

863 **Conkling, M., Hesp, K., Munroe, S., Sandoval, K., Martens, D. E., Sipkema, D., Wijffels, R. H. and**
864 **Pomponi, S. A.** (2019). Breakthrough in Marine Invertebrate Cell Culture: Sponge Cells Divide
865 Rapidly in Improved Nutrient Medium. *Scientific Reports* **9**.

866 **Core Team** (2013). R: A language and environment for statistical computing. *R Foundation for Statistical*
867 *Computing*, Vienna, Austria. URL <http://www.R-project.org/>.

868 **Custodio, M. R., Prokic, I., Steffen, R., Koziol, C., Borojevic, R., Brümmer, F., Nickel, M. and Müller, W.**
869 **E.** (1998). Primmorphs generated from dissociated cells of the sponge *Suberites domuncula*: a
870 model system for studies of cell proliferation and cell death. *Mech. Ageing Dev.* **105**, 45–59.

871 **Daley, A. C. and Antcliffe, J. B.** (2019). Evolution: The Battle of the First Animals. *Current Biology* **29**,
872 R257–R259.

873 **Deerinck, T. J., Bushong, E., Thor, A. and Ellisman, M. H.** (2010). NCMIR methods for 3D EM: A new
874 protocol for preparation of biological specimens for serial block-face SEM. *Microscopy*, 6-8.
875
876

877 **Dunn, C. W., Leys, S. P. and Haddock, S. H. D.** (2015). The hidden biology of sponges and ctenophores.
878 *Trends in Ecology & Evolution* **30**, 282–291.

879 **Elliott, G. R. D. and Leys, S. P.** (2007). Coordinated contractions effectively expel water from the
880 aquiferous system of a freshwater sponge. *Journal of Experimental Biology* **210**, 3736–3748.

881 **Elliott, G. R. D. and Leys, S. P.** (2010). Evidence for glutamate, GABA and NO in coordinating behaviour
882 in the sponge, *Ephydatia muelleri* (Demospongiae, Spongillidae). *J. Exp. Biol.* **213**, 2310–2321.

883 **Ellwanger, K. and Nickel, M.** (2006). Neuroactive substances specifically modulate rhythmic body
884 contractions in the nerveless metazoon *Tethya wilhelma* (Demospongiae, Porifera). *Front. Zool.*
885 **3**, 7.

886 **Ellwanger, K., Eich, A. and Nickel, M.** (2007). GABA and glutamate specifically induce contractions in the
887 sponge *Tethya wilhelma*. *J. Comp. Physiol. A Neuroethol. Sens. Neural. Behav. Physiol.* **193**, 1–
888 11.

889 **Ereskovsky, A. V.** (2010). *The Comparative Embryology of Sponges*. Dordrecht: Springer Netherlands.

890 **Ereskovsky, A. V. and Tokina, D. B.** (2007). Asexual reproduction in homoscleromorph sponges
891 (Porifera; Homoscleromorpha). *Marine Biology* **151**, 425–434.

892 **Ereskovsky, A. V., Tokina, D. B., Bézac, C. and Boury-Esnault, N.** (2007). Metamorphosis of
893 cinctoblastula larvae (Homoscleromorpha, porifera). *Journal of Morphology* **268**, 518–528.

894 **Ereskovsky, A. V., Borchellini, C., Gazave, E., Ivanisevic, J., Lapébie, P., Perez, T., Renard, E. and**
895 **Vacelet, J.** (2009). The Homoscleromorph sponge *Oscarella lobularis*, a promising sponge model
896 in evolutionary and developmental biology. *Bioessays* **31**, 89–97.

897 **Ereskovsky, A. V., Dubois, M., Ivanišević, J., Gazave, E., Lapebie, P., Tokina, D. and Pérez, T.** (2013a).
898 Pluri-annual study of the reproduction of two Mediterranean *Oscarella* species (Porifera,
899 Homoscleromorpha): cycle, sex-ratio, reproductive effort and phenology. *Marine Biology* **160**,
900 423–438.

901 **Ereskovsky, A., Renard, E. and Borchellini, C.** (2013b). Cellular and molecular processes leading to
902 embryo formation in sponges: evidences for high conservation of processes throughout animal
903 evolution. *Development Genes and Evolution* **223**, 5–22.

904 **Ereskovsky, A. V., Borisenko, I. E., Lapébie, P., Gazave, E., Tokina, D. B. and Borchellini, C.** (2015).
905 *Oscarella lobularis* (Homoscleromorpha, Porifera) Regeneration: Epithelial Morphogenesis and
906 Metaplasia. *PLOS ONE* **10**, e0134566.

907 **Erives, A. and Fritzsch, B.** (2019). A Screen for Gene Paralogies Delineating Evolutionary Branching Order
908 of Early Metazoa. *G3 (Bethesda)* **10**, 811–826.

909 **Fierro-Constain, L.** (2016). La reproduction chez *Oscarella lobularis* (Porifera - Homoscleromorpha) :
910 gènes impliqués et effets de l’environnement. <http://www.theses.fr>.

911 **Fierro-Constain, L., Schenkelaars, Q., Gazave, E., Haguenaer, A., Rocher, C., Ereskovsky, A.,**
912 **Borchellini, C. and Renard, E.** (2017). The Conservation of the GermLine Multipotency Program,
913 from Sponges to Vertebrates: A Stepping Stone to Understanding the Somatic and GermLine
914 Origins. *Genome Biol Evol* **9**, 474–488.

915 **Fernandez-Valverde, S. L., Calcino, A. D. and Degnan, B. M.** (2015). Deep developmental transcriptome
916 sequencing uncovers numerous new genes and enhances gene annotation in the sponge
917 *Amphimedon queenslandica*. *BMC Genomics* **16**.

918 **Fortunato, S., Adamski, M., Bergum, B., Guder, C., Jordal, S., Leininger, S., Zwafink, C., Rapp, H. T. and**
919 **Adamska, M.** (2012). Genome-wide analysis of the sox family in the calcareous sponge *Sycon*
920 *ciliatum*: multiple genes with unique expression patterns. *EvoDevo* **3**, 14.

921 **Fortunato, S. A. V., Adamski, M., Ramos, O. M., Leininger, S., Liu, J., Ferrier, D. E. K. and Adamska, M.**
922 (2014). Calcisponges have a ParaHox gene and dynamic expression of dispersed NK homeobox
923 genes. *Nature* **514**, 620–623.

924 **Fortunato, S. A. V., Adamski, M. and Adamska, M.** (2015). Comparative analyses of developmental
925 transcription factor repertoires in sponges reveal unexpected complexity of the earliest animals.
926 *Mar Genomics* **24 Pt 2**, 121–129.

927 **Funayama, N., Nakatsukasa, M., Hayashi, T. and Agata, K.** (2005). Isolation of the choanocyte in the
928 fresh water sponge, *Ephydatia fluviatilis* and its lineage marker, Ef annexin. *Dev. Growth Differ.*
929 **47**, 243–253.

930 **Gazave, E., Lapébie, P., Renard, E., Bézac, C., Boury-Esnault, N., Vacelet, J., Pérez, T., Manuel, M. and**
931 **Borchiellini, C.** (2008). NK homeobox genes with choanocyte-specific expression in
932 homoscleromorph sponges. *Development Genes and Evolution* **218**, 479–489.

933 **Gazave, E., Lapébie, P., Renard, E., Vacelet, J., Rocher, C., Ereskovsky, A. V., Lavrov, D. V. and**
934 **Borchiellini, C.** (2010). Molecular Phylogeny Restores the Supra-Generic Subdivision of
935 Homoscleromorph Sponges (Porifera, Homoscleromorpha). *PLOS ONE* **5**, e14290.

936 **Gazave, E., Lapébie, P., Ereskovsky, A. V., Vacelet, J., Renard, E., Cárdenas, P. and Borchiellini, C.**
937 (2012). No longer Demospongiae: Homoscleromorpha formal nomination as a fourth class of
938 Porifera. *Hydrobiologia* **687**, 3–10.

939 **Gazave, E., Lavrov, D. V., Cabrol, J., Renard, E., Rocher, C., Vacelet, J., Adamska, M., Borchiellini, C. and**
940 **Ereskovsky, A. V.** (2013). Systematics and molecular phylogeny of the family oscarellidae
941 (homoscleromorpha) with description of two new oscarella species. *PLoS ONE* **8**, e63976.

942 **Grant, N., Matveev, E., Kahn, A. S. and Leys, S. P.** (2018). Suspended sediment causes feeding current
943 arrests in situ in the glass sponge *Aphrocallistes vastus*. *Marine Environmental Research* **137**,
944 111–120.

945 **Gloeckner, V., Hentschel, U., Ereskovsky, A. V. and Schmitt, S.** (2013). Unique and species-specific
946 microbial communities in *Oscarella lobularis* and other Mediterranean *Oscarella* species
947 (Porifera: Homoscleromorpha). *Mar Biol* **160**, 781–791.

948 **Grasela, J. J., Pomponi, S. A., Rinkevich, B. and Grima, J.** (2012). Efforts to develop a cultured sponge
949 cell line: revisiting an intractable problem. *In Vitro Cellular & Developmental Biology. Animal* **48**,
950 12–20.

951 **Grice, L. F., Gauthier, M. E. A., Roper, K. E., Fernàndez-Busquets, X., Degnan, S. M. and Degnan, B. M.**
952 (2017). Origin and Evolution of the Sponge Aggregation Factor Gene Family. *Mol Biol Evol* **34**,
953 1083–1099.

954 **Hall, C., Rodriguez, M., Garcia, J., Posfai, D., DuMez, R., Wictor, E., Quintero, O. A., Hill, M. S., Rivera,**
955 **A. S. and Hill, A. L.** (2019). Secreted frizzled related protein is a target of PaxB and plays a role
956 in aquiferous system development in the freshwater sponge, *Ephydatia muelleri*. *PLoS ONE* **14**,
957 e0212005.

958 **Hammel, J. U. and Nickel, M.** (2014). A New Flow-Regulating Cell Type in the Demosponge *Tethya*
959 *wilhelma* – Functional Cellular Anatomy of a Leuconoid Canal System. *PLOS ONE* **9**, e113153.

960 **Heasman, J.** (2002). Morpholino Oligos: Making Sense of Antisense? *Developmental Biology* **243**, 209–
961 214.

962 **Imsiecke, G., Custodio, M., Borojevic, R., Steffen, R., Moustafa, M. A. and Müller, W. E. G.** (1995).
963 Genome size and chromosomes in marine sponges [*Suberites domuncula*, *Geodia cydonium*].
964 *Cell Biology International* **19**, 995–1000.

965 **Ishijima, J., Iwabe, N., Masuda, Y., Watanabe, Y. and Matsuda, Y.** (2008). Sponge cytogenetics - mitotic
966 chromosomes of ten species of freshwater sponge. *Zool. Sci.* **25**, 480–486.

967 **Johnston, I. S. and Hildemann, W. H.** (1982). Cellular organization in the marine demosponge
968 *Callyspongia diffusa*. *Mar. Biol.* **67**, 1–7.

969 **Jourda, C., Santini, S., Rocher, C., Le Bivic, A. and Claverie, J.-M.** (2015). Draft Genome Sequence of an
970 Alphaproteobacterium Associated with the Mediterranean Sponge *Oscarella lobularis*. *Genome*
971 *Announc* **3**.

972 **Kahn, A. S. and Leys, S. P.** (2016). The role of cell replacement in benthic–pelagic coupling by suspension
973 feeders. *R Soc Open Sci* **3**.

974 **King, N. and Rokas, A.** (2017). Embracing Uncertainty in Reconstructing Early Animal Evolution. *Current*
975 *Biology* **27**, R1081–R1088.

976 **Lai, A. G. and Aboobaker, A. A.** (2018). EvoRegen in animals: Time to uncover deep conservation or
977 convergence of adult stem cell evolution and regenerative processes. *Dev. Biol.* **433**, 118–131.

978 **Lanna, E.** (2015). Evo-devo of non-bilaterian animals. *Genet Mol Biol* **38**, 284–300.

979 **Leininger, S., Adamski, M., Bergum, B., Guder, C., Liu, J., Laplante, M., Bråte, J., Hoffmann, F.,**
980 **Fortunato, S., Jordal, S., et al.** (2014). Developmental gene expression provides clues to
981 relationships between sponge and eumetazoan body plans. *Nature Communications* **5**,
982 ncomms4905.

983 **Lapébie, P., Gazave, E., Ereskovsky, A., Derelle, R., Bézac, C., Renard, E., Houliston, E. and Borchellini,**
984 **C.** (2009). WNT/ β -Catenin Signalling and Epithelial Patterning in the Homoscleromorph Sponge
985 Oscarella. *PLOS ONE* **4**, e5823.

986 **Latifkar, A., Hur, Y. H., Sanchez, J. C., Cerione, R. A. and Antonyak, M. A.** (2019). New insights into
987 extracellular vesicle biogenesis and function. *J Cell Sci* **132**.

988 **Laumer, C. E., Fernández, R., Lemer, S., Combosch, D., Kocot, K. M., Riesgo, A., Andrade, S. C. S.,**
989 **Sterr, W., Sørensen, M. V. and Giribet, G.** (2019). Revisiting metazoan phylogeny with
990 genomic sampling of all phyla. *Proc. Biol. Sci.* **286**, 20190831.

991 **Lavrov, A. I. and Kosevich, I. A.** (2014). Sponge cell reaggregation: Mechanisms and dynamics of the
992 process. *Russ J Dev Biol* **45**, 205–223.

993 **Lavrov, A. I. and Kosevich, I. A.** (2016). Sponge cell reaggregation: Cellular structure and morphogenetic
994 potencies of multicellular aggregates. *J Exp Zool A Ecol Genet Physiol* **325**, 158–177.

995 **Lavrov, A. I., Bolshakov, F. V., Tokina, D. B. and Ereskovsky, A. V.** (2018). Sewing up the wounds: The
996 epithelial morphogenesis as a central mechanism of calcaronean sponge regeneration. *J. Exp.*
997 *Zool. B Mol. Dev. Evol.* **330**, 351–371.

998 **Leys, S. P.** (2015). Elements of a “nervous system” in sponges. *Journal of Experimental Biology* **218**, 581–
999 591.

1000 **Leys, S. P. and Degnan, B. M.** (2001). Cytological basis of photoresponsive behavior in a sponge larva.
1001 *Biol. Bull.* **201**, 323–338.

1002 **Leys, S. P. and Meech, R. W.** (2006). Physiology of coordination in sponges. *Canadian Journal of Zoology*
1003 **84**, 288–306.

1004 **Leys, S. P., Mackie, G. O. and Meech, R. W.** (1999). Impulse conduction in a sponge. *J. Exp. Biol.* **202 (Pt**
1005 **9)**, 1139–1150.

1006 **Leys, S. P., Cronin, T. W., Degnan, B. M. and Marshall, J. N.** (2002). Spectral sensitivity in a sponge larva.
1007 *J. Comp. Physiol. A Neuroethol. Sens. Neural. Behav. Physiol.* **188**, 199–202.

1008 **Leys, S. P., Nichols, S. A. and Adams, E. D. M.** (2009). Epithelia and integration in sponges. *Integrative*
1009 *and Comparative Biology* **49**, 167–177.

1010 **Leys, S. P., Yahel, G., Reidenbach, M. A., Tunncliffe, V., Shavit, U. and Reiswig, H. M.** (2011). The
1011 Sponge Pump: The Role of Current Induced Flow in the Design of the Sponge Body Plan. *PLoS*
1012 *ONE* **6**, e27787.

1013 **Leys, S. P., Mah, J. L., McGill, P. R., Hamonic, L., De Leo, F. C. and Kahn, A. S.** (2019). Sponge Behavior
1014 and the Chemical Basis of Responses: A Post-Genomic View. *Integr. Comp. Biol.* **59**, 751–764.

1015 **Ludeman, D. A., Farrar, N., Riesgo, A., Paps, J. and Leys, S. P.** (2014). Evolutionary origins of sensation
1016 in metazoans: functional evidence for a new sensory organ in sponges. *BMC Evol Biol* **14**, 3.

1017 **Mah, J. L. and Leys, S. P.** (2017). Think like a sponge: The genetic signal of sensory cells in sponges. *Dev.*
1018 *Biol.* **431**, 93–100.

1019 **Mah, J. L., Christensen-Dalsgaard, K. K. and Leys, S. P.** (2014). Choanoflagellate and choanocyte collar-
1020 flagellar systems and the assumption of homology. *Evolution & Development* **16**, 25–37.

1021 **Maldonado, M.** (2006). The ecology of the sponge larva. *Canadian Journal of Zoology* **84**, 175–194.

1022 **Maldonado, M., Durfort, M., McCarthy, D. A. and Young, C. M.** (2003). The cellular basis of
1023 photobehavior in the tufted parenchymella larva of demosponges. *Marine Biology* **143**, 427–
1024 441.

1025 **Maldonado, M., Cortadellas, N., Trillas, M. I. and Rützler, K.** (2005). Endosymbiotic Yeast Maternally
1026 Transmitted in a Marine Sponge. *Biological Bulletin* **209**, 94–106.

1027 **Margolis, L. and Sadovsky, Y.** (2019). The biology of extracellular vesicles: The known unknowns. *PLOS*
1028 *Biology* **17**, e3000363.

1029 **Miller, P. W., Pokutta, S., Mitchell, J. M., Chodaparambil, J. V., Clarke, D. N., Nelson, W. J., Weis, W. I.**
1030 **and Nichols, S. A.** (2018). Analysis of a vinculin homolog in a sponge (phylum Porifera) reveals
1031 that vertebrate-like cell adhesions emerged early in animal evolution. *J. Biol. Chem.* **293**, 11674–
1032 11686.

1033 **Mulcahy, L. A., Pink, R. C. and Carter, D. R. F.** (2014). Routes and mechanisms of extracellular vesicle
1034 uptake. *J Extracell Vesicles* **3**.

1035 **Musser, J. M., Schippers, K. J., Nickel, M., Mizzon, G., Kohn, A. B., Pape, C., Hammel, J. U., Wolf, F.,**
1036 **Liang, C., Hernández-Plaza, A., et al.** (2019). Profiling cellular diversity in sponges informs animal
1037 cell type and nervous system evolution. *bioRxiv* 758276.

1038 **Nakanishi, N., Sogabe, S. and Degnan, B. M.** (2014). Evolutionary origin of gastrulation: insights from
1039 sponge development. *BMC Biol.* **12**, 26.

1040 **Nakayama, S., Arima, K., Kawai, K., Mohri, K., Inui, C., Sugano, W., Koba, H., Tamada, K., Nakata, Y. J.,**
1041 **Kishimoto, K., et al.** (2015). Dynamic Transport and Cementation of Skeletal Elements Build Up
1042 the Pole-and-Beam Structured Skeleton of Sponges. *Curr. Biol.* **25**, 2549–2554.

1043 **Nichols, S. A., Dirks, W., Pearse, J. S. and King, N.** (2006). Early evolution of animal cell signaling and
1044 adhesion genes. *Proc. Natl. Acad. Sci. U.S.A.* **103**, 12451–12456.

1045 **Nichols, S. A., Roberts, B. W., Richter, D. J., Fairclough, S. R. and King, N.** (2012). Origin of metazoan
1046 cadherin diversity and the antiquity of the classical cadherin/ β -catenin complex. *Proc Natl Acad*
1047 *Sci U S A* **109**, 13046–13051.

1048 **Nickel, M.** (2010). Evolutionary emergence of synaptic nervous systems: what can we learn from the
1049 non-synaptic, nerveless Porifera? *Invertebrate Biology* **129**, 1–16.

1050 **Nickel, M., Scheer, C., Hammel, J. U., Herzen, J. and Beckmann, F.** (2011). The contractile sponge
1051 epithelium sensu lato – body contraction of the demosponge *Tethya wilhelma* is mediated by
1052 the pinacoderm. *Journal of Experimental Biology* **214**, 1692–1698.

1053 **Niel, G. van, D’Angelo, G. and Raposo, G.** (2018). Shedding light on the cell biology of extracellular
1054 vesicles. *Nat Rev Mol Cell Biol* **19**, 213–228.

1055 **Peña, J. F., Alié, A., Richter, D. J., Wang, L., Funayama, N. and Nichols, S. A.** (2016). Conserved
1056 expression of vertebrate microvillar gene homologs in choanocytes of freshwater sponges.
1057 *Evodevo* **7**, 13.

1058 **Pfannkuchen, M. and Brümmer, F.** (2009). Heterologous expression of DsRed2 in young sponges
1059 (Porifera). *Int. J. Dev. Biol.* **53**, 1113–1117.

1060 **Rady, H., Salem, S. and Ez El-Arab, M.** (2019). Primmorph extracts and mesohyls of marine sponges
1061 inhibit proliferation and migration of hepatocellular carcinoma cells in vitro. *Journal of*
1062 *Pharmaceutical Analysis*.

1063 **Raposo, G. and Stahl, P. D.** (2019). Extracellular vesicles: a new communication paradigm? *Nat Rev Mol*
1064 *Cell Biol* **20**, 509–510.

1065 **Raposo, G. and Stoorvogel, W.** (2013). Extracellular vesicles: Exosomes, microvesicles, and friends. *J Cell*
1066 *Biol* **200**, 373–383.

1067

1068 **Renard, E., Vacelet, J., Gazave, E., Lapébie, P., Borchellini, C. and Ereskovsky, A. V.** (2009). Origin of
1069 the neuro-sensory system: new and expected insights from sponges. *Integr Zool* **4**, 294–308.

1070 **Renard, E., Eve, G., Fierro-Constain, L., Schenkelaars, Q., A.V., E., Vacelet, J. V. and Borchellini, C. B.**
1071 (2013). Porifera (Sponges): Recent Knowledge and New Perspectives. In *Encyclopedia of life*
1072 *sciences*.

1073 **Renard, E., Leys, S. P., Wörheide, G. and Borchellini, C.** (2018). Understanding Animal Evolution: The
1074 Added Value of Sponge Transcriptomics and Genomics. *BioEssays* **40**,.

1075 **Revilla-I-Domingo, R., Schmidt, C., Zifko, C. and Raible, F.** (2018). Establishment of Transgenesis in the
1076 Demosponge *Suberites domuncula*. *Genetics* **210**, 435–443.

1077 **Rivera, A. S., Hammel, J. U., Haen, K. M., Danka, E. S., Cieniewicz, B., Winters, I. P., Posfai, D.,**
1078 **Wörheide, G., Lavrov, D. V., Knight, S. W., et al.** (2011). RNA interference in marine and
1079 freshwater sponges: actin knockdown in *Tethya wilhelma* and *Ephydatia muelleri* by ingested
1080 dsRNA expressing bacteria. *BMC Biotechnol* **11**, 67.

1081 **Rivera, A., Winters, I., Rued, A., Ding, S., Posfai, D., Cieniewicz, B., Cameron, K., Gentile, L. and Hill, A.**
1082 (2013). The evolution and function of the Pax/Six regulatory network in sponges. *Evol. Dev.* **15**,
1083 186–196.

1084 **Russell, J. J., Theriot, J. A., Sood, P., Marshall, W. F., Landweber, L. F., Fritz-Laylin, L., Polka, J. K.,**
1085 **Oliferenko, S., Gerbich, T., Gladfelter, A., et al.** (2017). Non-model model organisms. *BMC Biol*
1086 **15**.

1087 **Schenkelaars, Q., Quintero, O., Hall, C., Fierro-Constain, L., Renard, E., Borchiellini, C. and Hill, A. L.**
1088 (2016). ROCK inhibition abolishes the establishment of the aquiferous system in *Ephydatia*
1089 *muelleri* (Porifera, Demospongiae). *Dev. Biol.* **412**, 298–310.

1090 **Schenkelaars, Q., Vernale, A., Fierro-Constaín, L., Borchiellini, C. and Renard, E.** (2019). A Look Back
1091 Over 20 Years of Evo-Devo Studies on Sponges: A Challenged View of Urmetazoa. In *Evolution,*
1092 *Origin of Life, Concepts and Methods* (ed. Pontarotti, P.), pp. 135–160. Cham: Springer
1093 International Publishing.

1094 **Schill, R. O., Pfannkuchen, M., Fritz, G., Köhler, H.-R. and Brümmer, F.** (2006). Quiescent gemmules of
1095 the freshwater sponge, *Spongilla lacustris* (Linnaeus, 1759), contain remarkably high levels of
1096 Hsp70 stress protein and hsp70 stress gene mRNA. *J. Exp. Zoolog. Part A Comp. Exp. Biol.* **305**,
1097 449–457.

1098 **Schindelin, J., Arganda-Carreras, I., Frise, E., Kaynig, V., Longair, M., Pietzsch, T., Preibisch, S., Rueden,**
1099 **C., Saalfeld, S., Schmid, B., et al.** (2012). Fiji: an open-source platform for biological-image
1100 analysis. *Nat. Methods* **9**, 676–682.

1101 **Schippers, K. J., Nichols, S. A. and Wittkopp, P.** (2018). Evidence of Signaling and Adhesion Roles for β -
1102 Catenin in the Sponge *Ephydatia muelleri*. *Mol Biol Evol* **35**, 1407–1421.

1103 **Sebé-Pedrós, A., Chomsky, E., Pang, K., Lara-Astiaso, D., Gaiti, F., Mukamel, Z., Amit, I., Hejnol, A.,**
1104 **Degnan, B. M. and Tanay, A.** (2018). Early metazoan cell type diversity and the evolution of
1105 multicellular gene regulation. *Nature Ecology & Evolution* **2**, 1176–1188.

1106 **Simion, P., Philippe, H., Baurain, D., Jager, M., Richter, D. J., Di Franco, A., Roure, B., Satoh, N.,**
1107 **Quéinnec, É., Ereskovsky, A., et al.** (2017). A Large and Consistent Phylogenomic Dataset
1108 Supports Sponges as the Sister Group to All Other Animals. *Current Biology* **27**, 958–967.

1109 **Simpson, T. L.** (1984). *The cell biology of sponges*. New York: Springer-Verlag.

1110 **Sipkema, D., Snijders, A. P. L., Schroën, C. G. P. H., Osinga, R. and Wijffels, R. H.** (2004). The life and
1111 death of sponge cells. *Biotechnol. Bioeng.* **85**, 239–247.

1112 **Sogabe, S., Nakanishi, N. and Degnan, B. M.** (2016). The ontogeny of choanocyte chambers during
1113 metamorphosis in the demosponge *Amphimedon queenslandica*. *Evodevo* **7**, 6.

1114 **Sogabe, S., Hatleberg, W. L., Kocot, K. M., Say, T. E., Stoupin, D., Roper, K. E., Fernandez-Valverde, S.**
1115 **L., Degnan, S. M. and Degnan, B. M.** (2019). Pluripotency and the origin of animal
1116 multicellularity. *Nature* **570**, 519–522.

1117 **Srivastava, M., Simakov, O., Chapman, J., Fahey, B., Gauthier, M. E. A., Mitros, T., Richards, G. S.,**
1118 **Conaco, C., Dacre, M., Hellsten, U., et al.** (2010). The *Amphimedon queenslandica* genome and
1119 the evolution of animal complexity. *Nature* **466**, 720–726.

1120 **Ueda, N., Richards, G. S., Degnan, B. M., Kranz, A., Adamska, M., Croll, R. P. and Degnan, S. M.** (2016).
1121 An ancient role for nitric oxide in regulating the animal pelagobenthic life cycle: evidence from
1122 a marine sponge. *Sci Rep* **6**, 37546.

1123 **Voigt, O., Adamski, M., Sluzek, K. and Adamska, M.** (2014). Calcareous sponge genomes reveal complex
1124 evolution of α -carbonic anhydrases and two key biomineralization enzymes. *BMC Evol. Biol.* **14**,
1125 230.

1126 **Whelan, N. V., Kocot, K. M., Moroz, T. P., Mukherjee, K., Williams, P., Paulay, G., Moroz, L. L. and**
1127 **Halanych, K. M.** (2017). Ctenophore relationships and their placement as the sister group to all
1128 other animals. *Nature Ecology & Evolution* **1**.

1129 **Windsor, P. J. and Leys, S. P.** (2010). Wnt signaling and induction in the sponge aquiferous system:
1130 evidence for an ancient origin of the organizer. *Evol. Dev.* **12**, 484–493.

1131 **Windsor Reid, P. J., Matveev, E., McClymont, A., Posfai, D., Hill, A. L. and Leys, S. P.** (2018). Wnt
1132 signaling and polarity in freshwater sponges. *BMC Evolutionary Biology* **18**, 12.

1133 **Wong, E., Mölter, J., Anggono, V., Degnan, S. M. and Degnan, B. M.** (2019). Co-expression of synaptic
1134 genes in the sponge *Amphimedon queenslandica* uncovers ancient neural submodules. *Sci Rep*
1135 **9**, 15781.

1136 **Zeller, R. W., Virata, M. J. and Cone, A. C.** (2006). Predictable mosaic transgene expression in ascidian
1137 embryos produced with a simple electroporation device. *Developmental Dynamics* **235**, 1921–
1138 1932.

1139

1140

1141

1142

1143

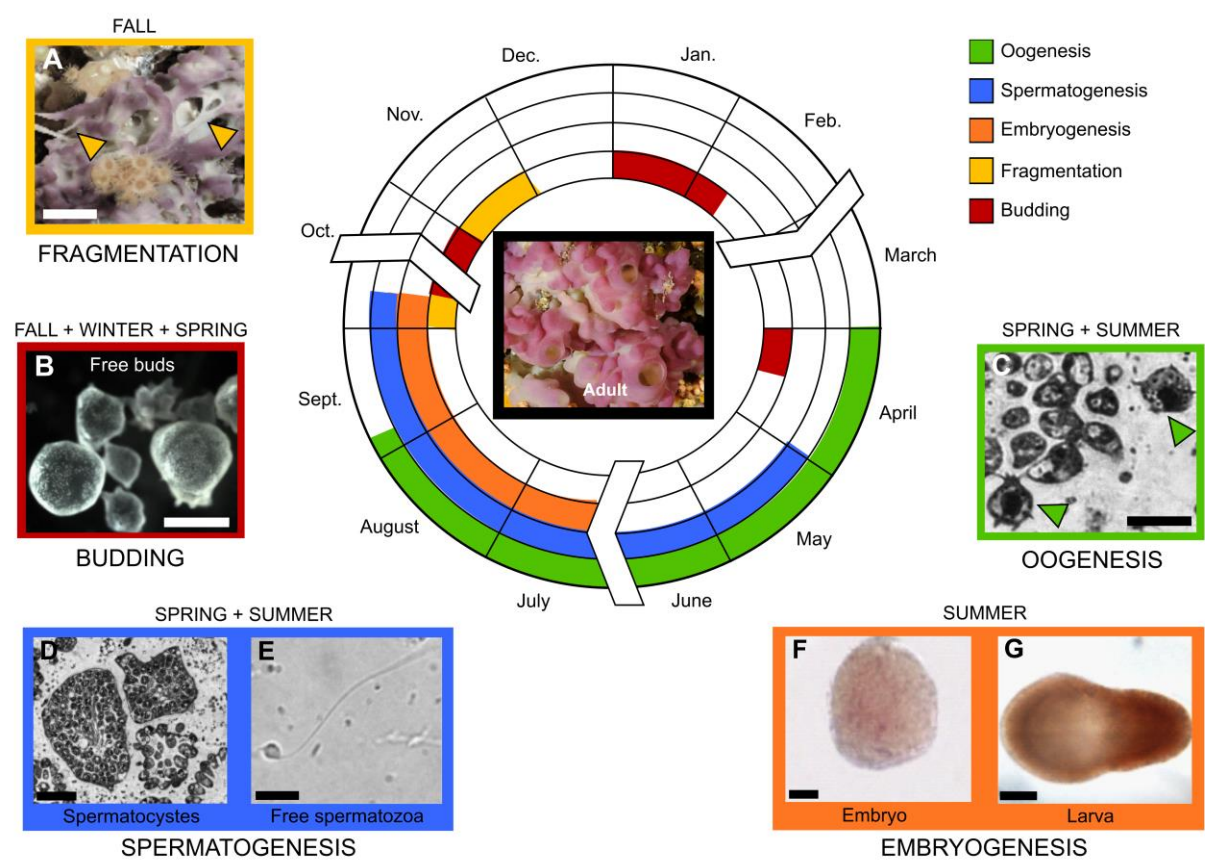


Fig. 1: Reproduction events during the life cycle of *Oscarella lobularis*. (A) Asexual reproduction by fragmentation (arrow heads) occurs at fall, scale bar 1cm. (B) Asexual reproduction by budding yields to the release of free-floating buds, scale bar 500µm. (C-G) Sexual reproduction takes place from April to October. (C) Oocytes (green arrows) near a choanocyte chamber, scale bar 8µm. (D) Spermatozoa in spermatocysts, scale bar 25µm. (E) Released spermatozoa, scale bar 2µm. (F) Embryo dissected from maternal tissues, scale bar 50µm. (G) Swimming larva, scale bar 150µm (modified from Fierro-Constain (2016)).

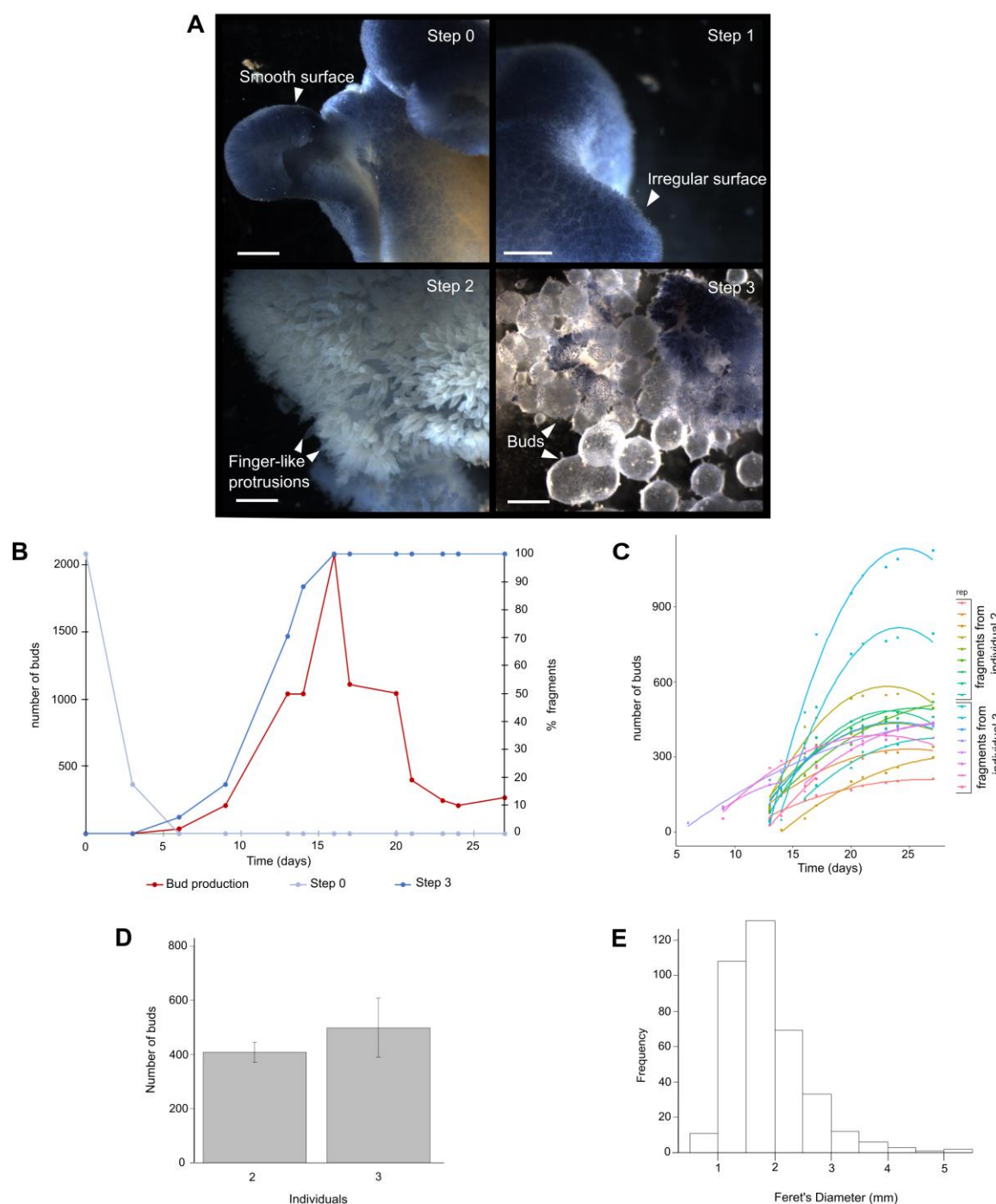
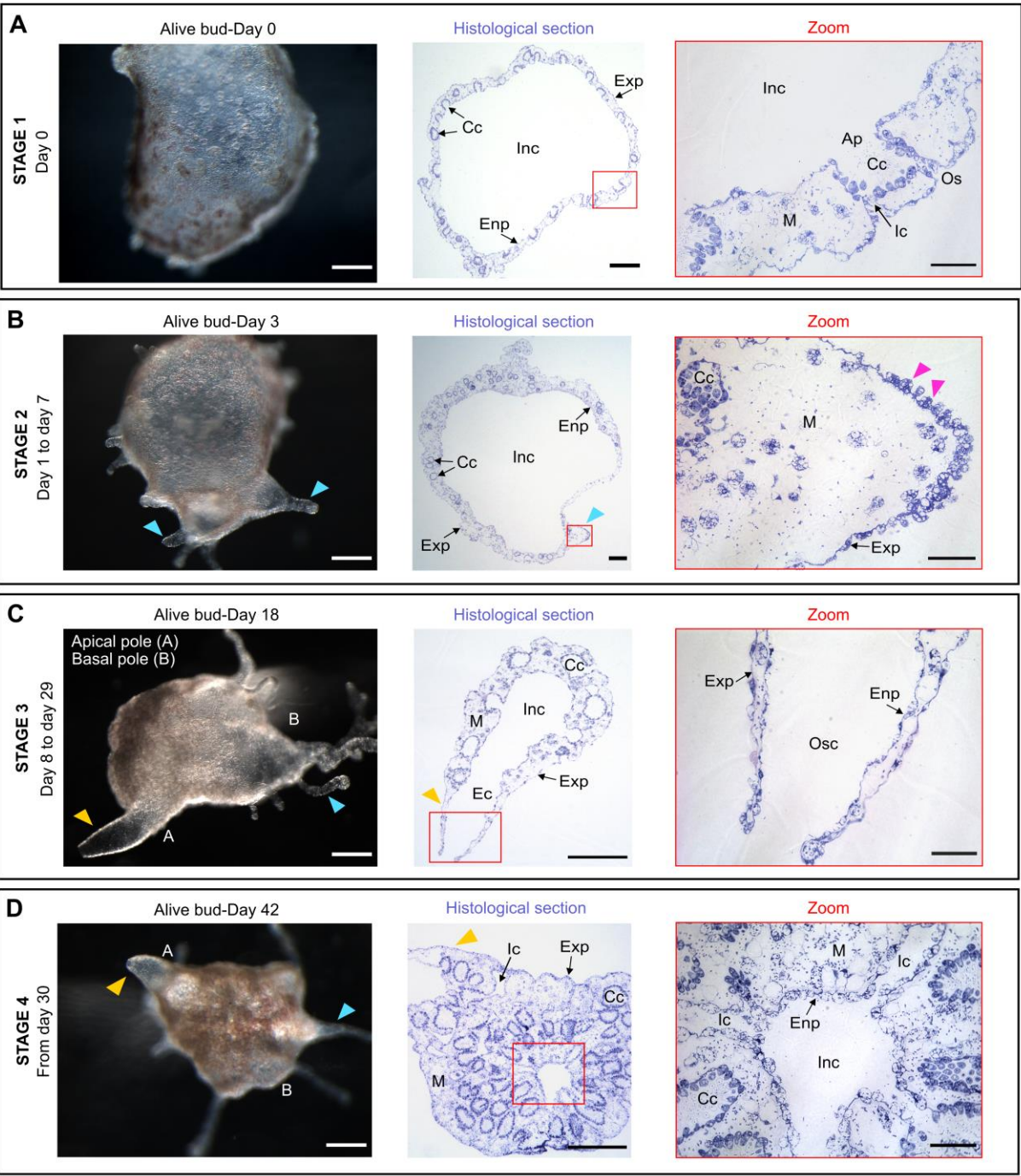


Fig. 2: Kinetics of budding and of bud release. (A) Alive *Oscarella lobularis* fragments and buds observed using a stereo microscope; Step 0: smooth surface of a freshly sampled individual; Step 1: the surface becomes irregular; Step2: the surface is covered by finger-like protrusions; Step 3: The swelling up of protrusions results in the formation of buds that are subsequently released; Scale bars: 1mm. (B) Kinetics of budding (Table S1), budding starts 6 days after cutting and reaches a peak of bud release between 13th and 16th days after the beginning of budding process (red curve). The bud production is correlated with the percentage of fragments that reached the third step of the budding process (blue curve). (C) Daily release (cumulative) of new buds per fragment (17 fragments from two individuals) (see Table S2). (D) Average bud production for each of the 2 monitored individuals (mean: 451.4, sd: 225.56). (E) Size of stage 1 buds (Feret's Diameter (mm)); the diameter of 84% of the bud's ranges from 1 and 2.5 mm (mean: 1.87 mm, sd: 0.696 mm).



1170
1171 **Fig. 3: Development of bud.** (A) Stage 1: Spherical just-released Bud. (B) Stage 2: Bud with
1172 outgrowths (blue arrows) devoid of choanocyte chambers (zoom in) and with distal roundish
1173 cells (pink arrows). (C) Stage 3: bud with osculum (yellow arrows) and outgrowths (blue arrows)
1174 clustered on the opposite pole. (D) Stage 4: The juvenile in settled thanks to basopinacocytes
1175 and has a reduced internal cavity (atrium). Scale bars: 200µm (first column), 100µm (middle
1176 column), 20µm (zoom). Ap: apopyle; Cc: choanocyte chamber; Ec: exhalant canal; Enp:
1177 endopinacoderm; Exp: exopinacoderm; Ic: inhalant canal; Inc: Internal cavity; M: mesohyl; Osc:
1178 osculum; Os: ostium.

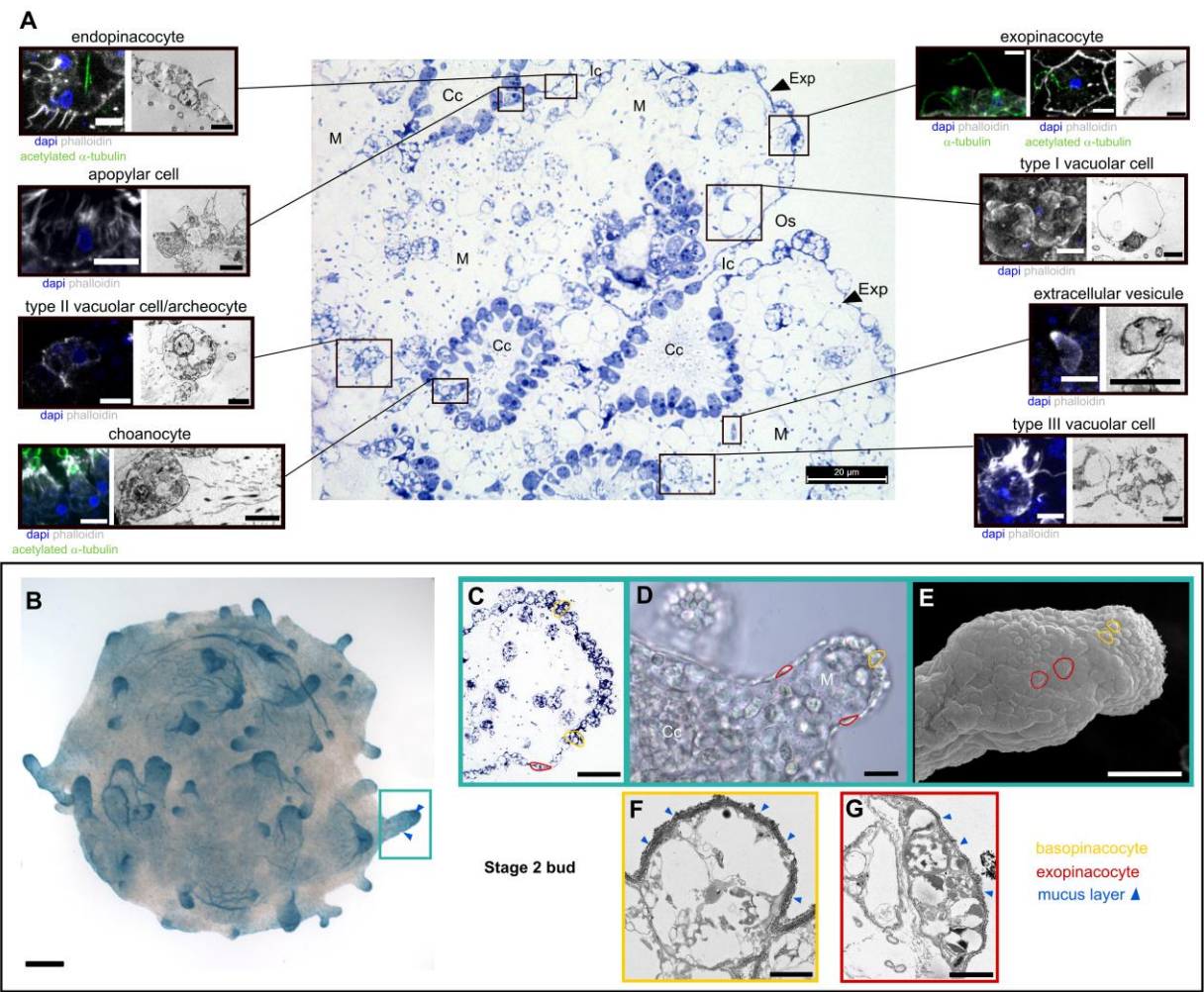


Fig. 4: Cell types of *Oscarella lobularis* buds. (A) Position of each cell types in the tissues observed on histological sections. For each cell type, the left picture is a max intensity projection of confocal Z-stack, scale bar: 5 μ m; on the right a TEM picture, scale bar: 2,5 μ m. (B) External view of a stage 2 bud showing accumulation of mucus (Alcian blue staining) at the distal part of the outgrowths (blue arrows). (C, D, E) Observations of stage 2 bud outgrowth on (C) semi-thin histological section, (D) white light microscopy and (E) MEB, showing the difference between flat exopinacocytes and roundish basopinacocytes. (F) Basopinacocytes (TEM) covered by thicker mucus layer (blue arrows) than exopinacocytes (TEM) (G). Scale bars: 100 μ m (B); 20 μ m (C,D); 43 μ m (E); 2 μ m (F,G). Cc: choanocyte chamber; Inc: internal cavity; Ic: inhalant canal; Exp: endopinacoderm; Exp: exopinacoderm; M: mesohyl; Os: ostium.

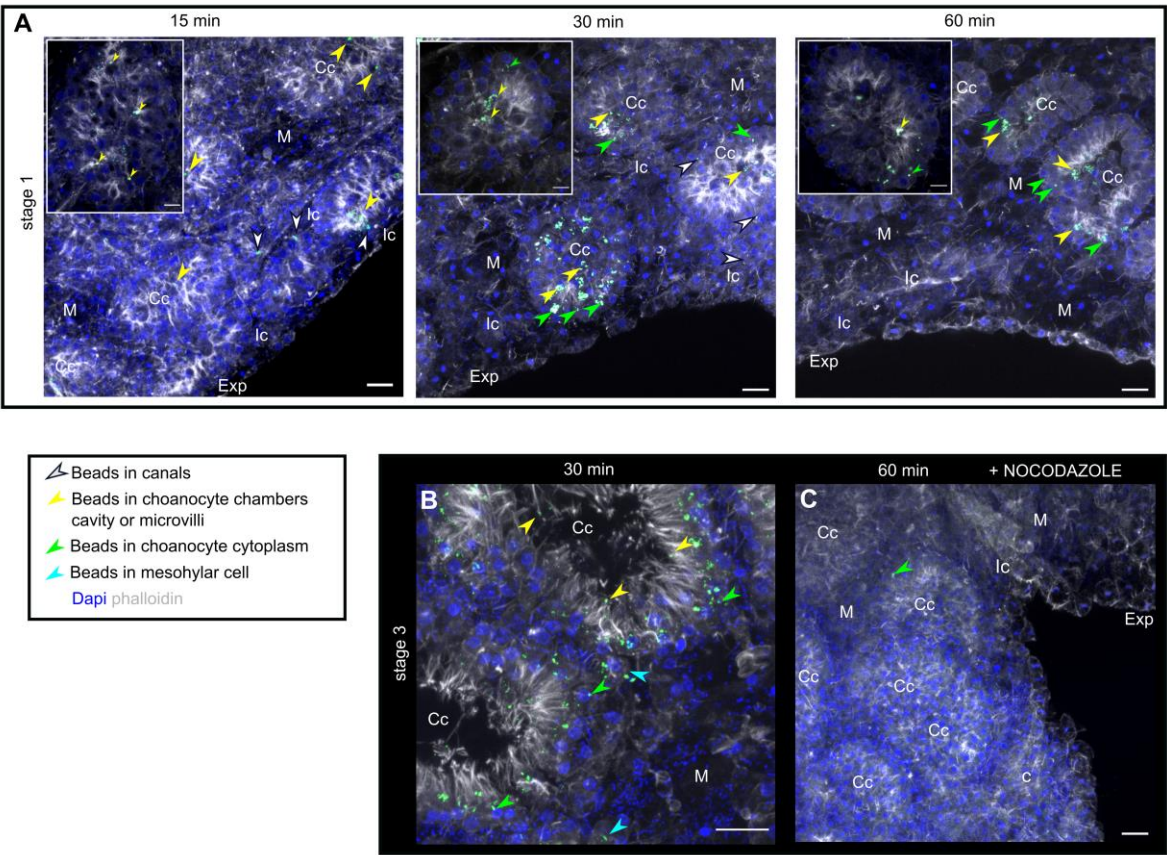
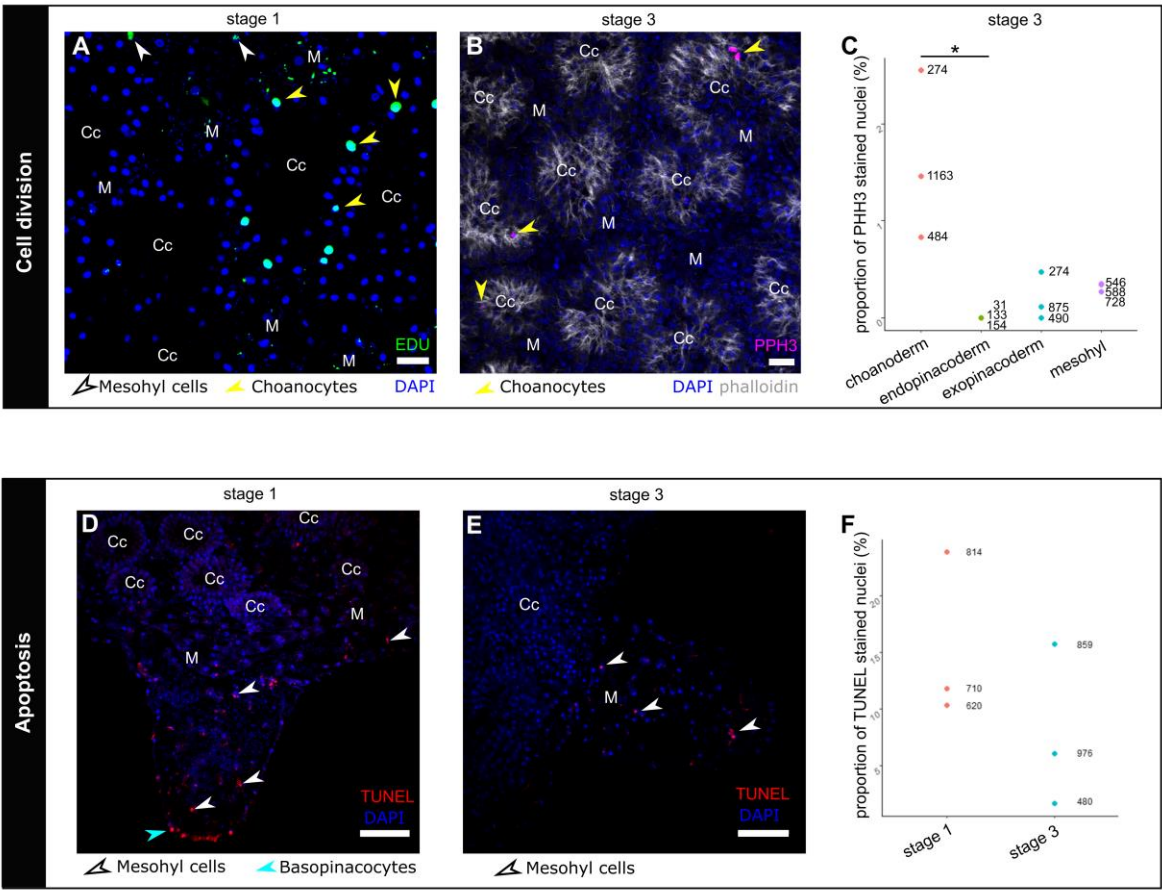


Fig. 5: Active filtering activity of buds evidenced by 0.2 μm fluorescent beads. (A) Location of beads in stage 1 buds (devoid of osculum) after 15, 30- and 60-min incubation with beads. Arrows of different colors show different locations: canals, choanocyte chambers cavity or microvilli, choanocyte cytoplasm and mesohylar cell cytoplasm. (B) Location of beads in stage 3 buds (with osculum) after 30 min incubation with beads, in choanocytes microvilli or choanocyte cytoplasm and in mesohylar cells. (C) Absence of filtering activity after a nocodazole treatment (near absence of beads in stage 3 buds after 60 min incubation) (control: DMSO treatment, Fig. S4). Scale bar: 10 μm (A,B,C). Cc: choanocyte chamber; Exp: exopinacoderm; Ic: inhalant canal; M: mesohyl. Max intensity projection of confocal Z-stack (A, B, C).



1214
1215 **Fig. 6: Cell renewing during bud development.** (A) Cell proliferation (green: EDU) concerns
1216 mainly choanocytes (yellow arrows) and, in less extent, mesohylar cells (white arrows), at stage
1217 1 (Table S5). (B) Cell proliferation (magenta: PHH3) also mainly concerns choanocytes at stage
1218 3. (C) Proportion of cells observed simultaneously in division by PHH3 immunostaining at stage
1219 3 (Table S6). Each dot represents the proportion observed for one sample, numbers indicate
1220 the total number of nuclei observed. Cell division is rarely observed in exopinacocytes (Fig.
1221 S5A,B,C) and has never been observed in endopinacocytes. The difference is significant (*)
1222 between choanocytes and endopinacocytes (Kruskall-Wallis: pvalue=0.0973; Dunn test:
1223 padj=0.0197). (D) TUNEL staining (red) at stage 1: apoptotic DNA fragmentation is mainly
1224 observed in basopinacocytes (cyan arrow) and in cells localized in the mesohyl (white arrows),
1225 (control: Fig. S5D). (E) TUNEL staining (red) at stage 3 in mesohylar cells (white arrows), in
1226 bacteria and extracellular vesicles (EVs) (Fig. S5E). (F) The proportion of cells undergoing
1227 apoptosis is not significantly different between stages 1 and 3 (values in Table S7), each dot
1228 represents the proportion observed for one sample, numbers indicate the total number of
1229 nuclei observed. Scale bars: 10µm (A, B); 30µm (D, E). Cc: choanocyte chamber; M: mesohyl.
1230 Max intensity projection of confocal Z-stack (D, E).

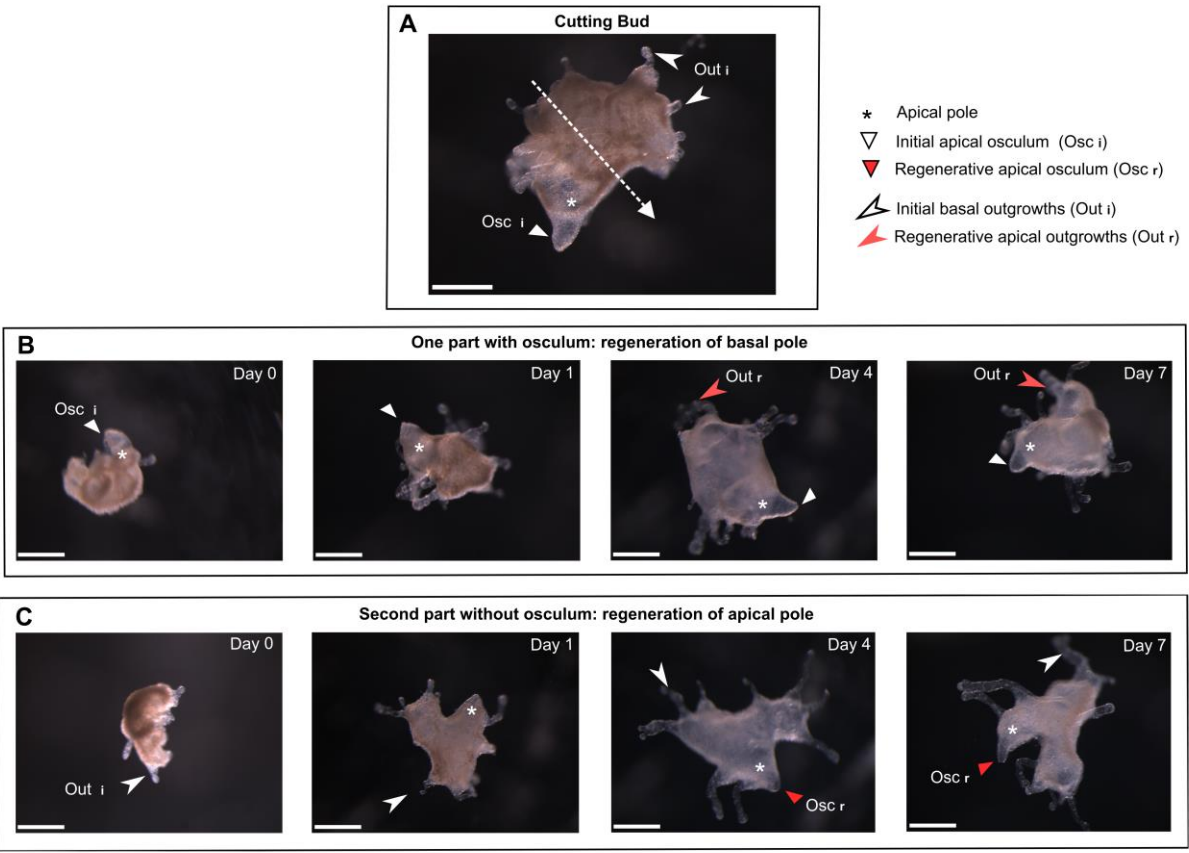


Fig. 7: Regenerative experiments. (A) Stage 3 bud with osculum at apical pole and outgrowths at basal pole. The dotted arrow represents the section level. (B) One half with primary osculum at apical pole and devoid of basal outgrowths and (C) one half without osculum but with basal outgrowths; After 96 h, both halves regenerate the missing part: new secondary osculum or new basal outgrowth. Scale bar: 500µm (A-C).

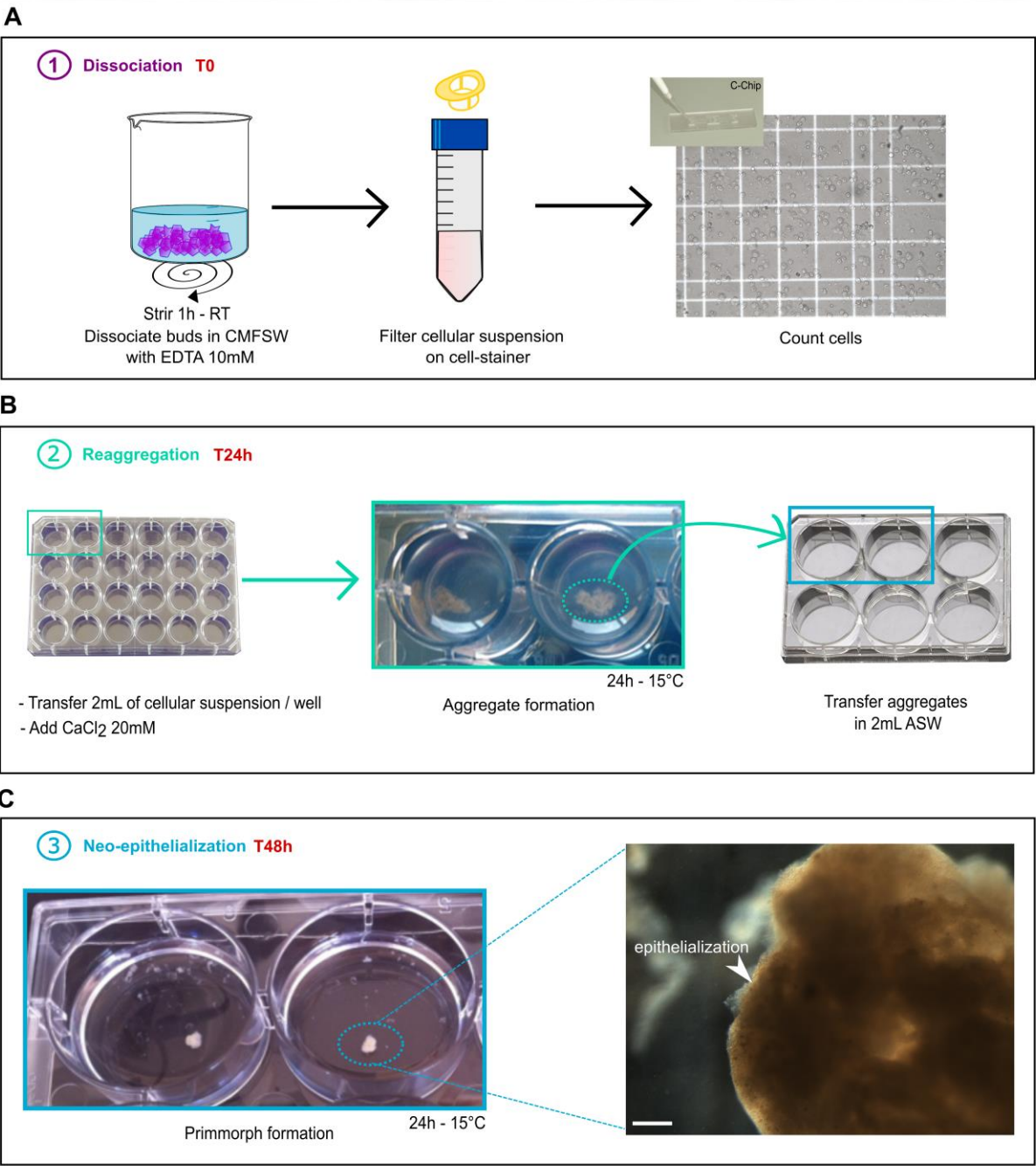


Fig. 8: Reaggregation of dissociated cells. (A) Buds are dissociated in CMFSW and EDTA to obtain a cell suspension. (B) 24h after the addition of calcium chloride, compact aggregates are observed. (C) After 48h in ASW, Primmorph are obtained, scale bar 50µm.

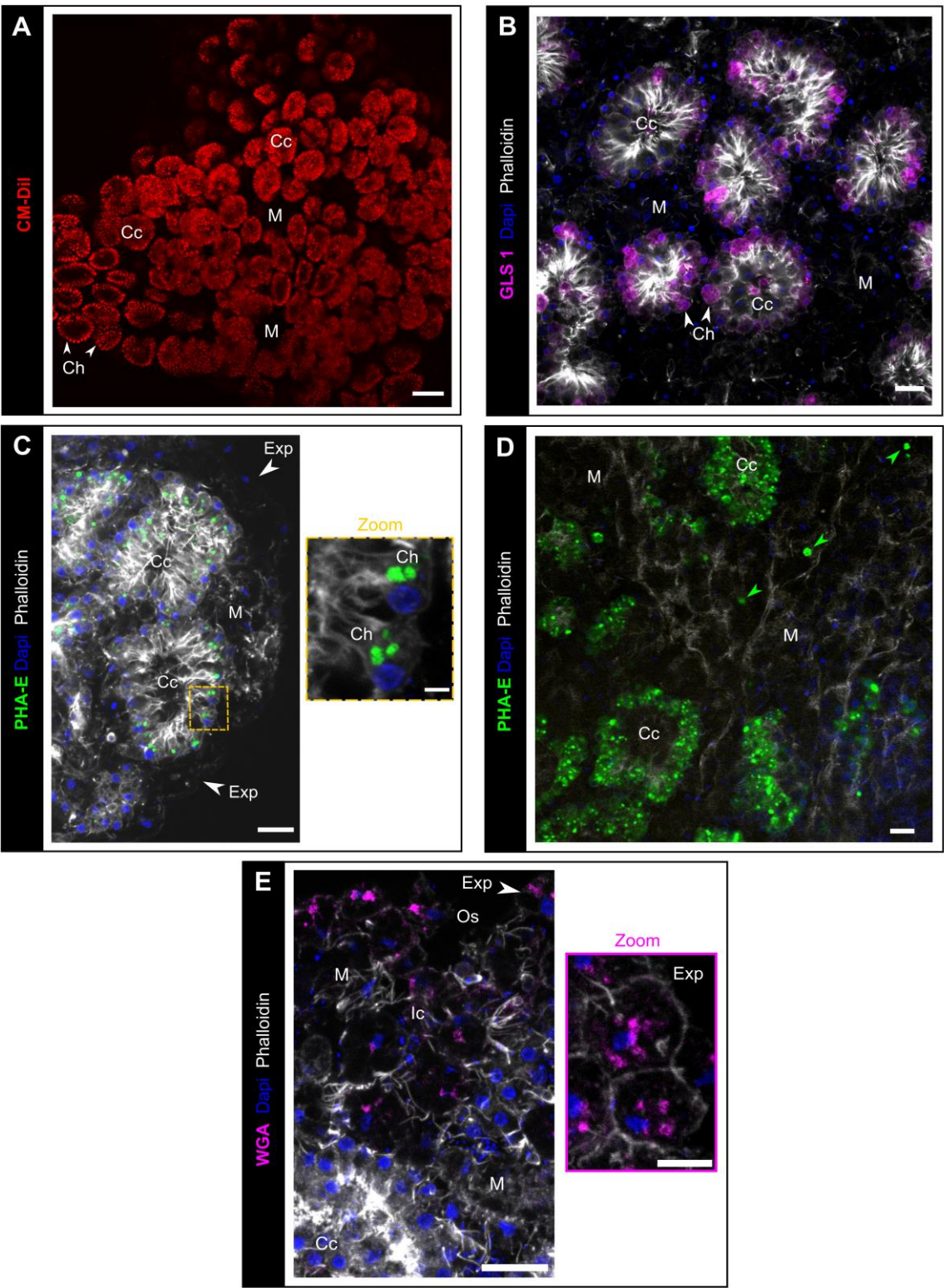


Fig. 9: Cell staining and tracking. (A) Observation (biphotonic microscope) of choanocyte chambers in alive bud labelled by the lipidic marker CM-Dil (red). (B) GSL1 lectin (magenta) staining of choanocytes (white arrows). (C) PhaE lectin staining of choanocytes (green). (D) The presence of PhaE-stained cells in the mesohyl (green arrows) indicates a transdifferentiation from choanocytes to mesohylar cells, after 72h regeneration. (E) Rhodamine-WGA (magenta) staining of exopinacocytes (white arrow). Scale bars: 50µm (A); 10µm (B-E); 2µm (Zoom C); 5µm (Zoom E). Ap: apopyle; Cc: choanocyte chamber; Ch: choanocyte, Exp: exopinacocytes; Ic: inhalant canal; M: mesohyl; Osc: osculum. Max intensity projection of confocal Z-stack (B-E).

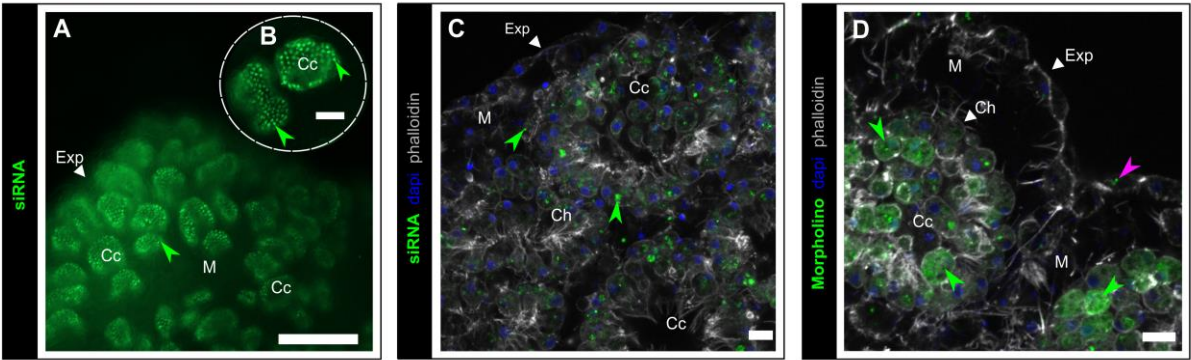


Fig. 10: Block-it siRNA and morpholino transfection in choanocytes. (A, B) Accumulation of BLOCK-iT™ fluorescent oligo (green) (incubation 72H at 8nM) in choanocyte chambers (green arrows), (epifluorescence microscope with X20 (A) and X40 (B) objectives). (C) BLOCK-iT™ (incubation 72h at 8nM) localized in choanocyte (green arrows). (D) Standard control morpholino (green) in choanocytes and in less extent in exopinacoderm (pink arrow). Scale bars: 100µm (A), 25µm (B), 7µm (C,D). Cc: choanocyte chamber; Ch: choanocyte; Exp: exopinacoderm; M: mesohyl. Max intensity projection of confocal Z-stack (C,D).

Table 1: Data and tools available for the main sponge species used for evo-devo studies (for review Schenkelaars et al., 2019)

species		environment	development in the lab	other morphogenetic experiments	Genome draft	transcriptome	Single cell transcriptomic	karyotype	In situ hybridization	immunofluorescence	Cell type specific staining	Live/Death staining	TUNEL staining	PH3/EDU/BrdU assays	pharmacological assays	Acid nucleic transfection	references
Homoscleromorpha	<i>Oscarella lobularis</i>	M	●	●	○	●	○	○	●	●	●	●	●	●	○		Belahbib et al 2018; Fierro-Constain et al., 2017; Gazave et al., 2008; Lapébie et al., 2009; Ereskovsky et al 2015; This paper
Demospongiae	<i>Amphimedon queenslandica</i>	M	●	●	●	●	●		●	●	●		●	●	●	○	Adamska et al., 2007; Fernandez-Valverde et al., 2015; Grice et al., 2017; Nakanishi et al., 2014; Sogabe et al., 2014, 2016, 2019; Ueda et al., 2016; Srivastava et al., 2010
	<i>Ephydatia muelleri</i>	F	●		●	●		●	●	●				●	●		Adams et al., 2010; Elliott and Leys, 2007; Imsiecke et al., 1995; Ishijima et al., 2008; Ludemann et al., 2014; Pena et al., 2016; Schenkelaars et al., 2016 ; Schippers et al., 2018; Rivera et al., 2011, 2013; Windsor and Leys, 2010; Winsor Reid et al., 2018; Hall et al., 2019
	<i>Ephydatia fluviatilis</i>	F	●			●	●	●	●		●	●		●	●		Alié et al., 2015;Funayama et al., 2005; Ishijima et al., 2008; Nakayama et al., 2015
	<i>Spongilla lacustris</i>	F	●		●	●	●	●	●		●				●		Adams et al., 2010; Kahn and Leys, 2016;Imsiecke et al., 1993; Ishijima et al., 2008; Mah et al., 2014; Pfannkuchen and Brummer, 2009; Schill et al., 2006; Windsor-reid et al., 2018
Calcarea	<i>Leucosolenia complicata</i>	M		●	●	●			●	●				●			Fortunato et al., 2015; Lavrov et al., 2018; Voigt et al., 2014
	<i>Sycon ciliatum</i>	M	●	●	●	●			●								Fortunato et al., 2012, 2014, 2015; Leininger et al., 2014; Voigt et al., 2014
Hexactinellida	<i>Aphrocallistes vastus</i>	M				●			●	●				●			Grant et al., 2018; kahn and Leys, 2016; Windsor-reid et al., 2018